TU/e EINDHOVEN UNIVERSITY OF TECHNOLOGY

Eindhoven University of Technology

MASTER

Optical studies of small metal particles

Gielkens, O.

Award date:
1995

Link to publication

Disclaimer
This document contains a student thesis (bachelor's or master's), as authored by a student at Eindhoven University of Technology. Student theses are made available in the TU/e repository upon obtaining the required degree. The grade received is not published on the document as presented in the repository. The required complexity or quality of research of student theses may vary by program, and the required minimum study period may vary in duration.

General rights
Copyright and moral rights for the publications made accessible in the public portal are retained by the authors and/or other copyright owners and it is a condition of accessing publications that users recognise and abide by the legal requirements associated with these rights.

- Users may download and print one copy of any publication from the public portal for the purpose of private study or research.
- You may not further distribute the material or use it for any profit-making activity or commercial gain

Optical studies of small metal particles

Olaf Gielkens

July 1995

Master Thesis

Surface and Interface Physics Group
Solid State Physics Division
Faculty of Applied Physics
Eindhoven University of Technology

Supervisor: DR. C.F.J. FLIPSE

Graduation Professor: PROF. DR. H.H. BRONGERSMA

Abstract

Upon reduction of the size of metal particles, changes can occur in the electron structure of these particles. Possible effects are a change in the plasma resonance frequency or even the disappearance of the plasma resonance when the particles become very small. Applying the spin-coat technique, highly dispersed small metal particles on a flat oxide substrate are prepared. Atomic Force Microscopy (AFM) is used to determine size and particle number density of the prepared particles. Spectroscopic ellipsometry is used to study the plasma resonance of gold and copper particles.

The plasma resonance was observed for large gold particles with a height of 40 nm, but not for small gold particles with a height of 4 nm. The absence of the resonance might be due to the particle size or to the fact that the particles have formed a thin film. The optical response of the small particles is similar to that of a gold monolayer, but it is not possible with AFM to determine the exact particle size and distribution of the small gold particles. For this, additional experiments are required.

Deposition of large copper particles resulted in agglomerates of particles. The total amount of copper deposited was too small to detect this with ellipsometry. The small copper particles with an average height of 10 nm, show no plasmon resonance. Possible reasons for this are the oxidation of the copper and the localisation of the conduction electrons.

Contents

1 Introduction **1**

2 Optical response of metal particles **3**
- 2.1 Electromagnetic Theory 3
- 2.2 Absorption Mechanisms 4
- 2.3 Surface Plasmons 6
- 2.4 Metal Particles 7

3 Ellipsometry **9**
- 3.1 General principles of ellipsometry 9
- 3.2 Simple models 10
  - 3.2.1 Impedance formalism 12
- 3.3 Enhanced surface and interface sensitivity 13
- 3.4 Instrumentation 15
  - 3.4.1 Ellipsometers in general 15
  - 3.4.2 Ellipsometer at the Philips Research Laboratories 16

4 Sample preparation and characterisation **19**
- 4.1 Preparation of nanometer-sized metal particles 19
  - 4.1.1 The spin-coat facility 21
- 4.2 Sample Characterisation 21
  - 4.2.1 Atomic Force Microscopy 21
  - 4.2.2 Electron Microscopy 23

5 Results **25**
- 5.1 Gold particles 25
- 5.2 Copper particles 34
- 5.3 Recommendations 39

References **41**

Dankwoord **43**

A Approximation of the molecular volume **44**

Chapter 1

Introduction

People have always been fascinated by the interaction of light with materials. The beautifull colours seen when light shines on a diamond, the existance of mirrors, rainbows and the red colour of the sky at sunset are just a few everyday-examples of this. The desire to understand the nature of this interaction between light and matter has been the motivation of a lot of research. This research was at first fundamental and just aimed at the understanding of the phenomena, but as people started to understand more and more, applications were soon developed. Examples of this are sunglasses, anti-reflection coatings, lasers and the transport of enormous amounts of data through just one small optical fiber.

Classically the optical properties of materials were described in terms of refractive indices and extinction coefficients. It is now understood that the optical properties of a material are defined by the electronic structure of the material and surface properties like roughness. For a lot of applications it is sufficient to know the optical properties of a material, the origin of these properties is not important. However, it is important to know the origin of the optical properties, as they serve as a guideline in the search for new materials with specific properties.

Small metal particles have been of interest for a long time. The optical behaviour of single particles as well as large collections of these particles have been the subject of a lot of studies. Most studies are related to the so-called surface plasmon resonance and its influence on non-linear optical properties of the particle. Recent research on these particles is directed to both applications and understanding of special properties of these particles. Haus *et al.* [1] for example, report on enhanced optical properties of metal-coated nanoparticles and refers to promising studies that concern small metal particles as compact polarisers for intergrated optics. Enhancement of non-linear optical properties, like second harmonic generation, due to the plasma resonance in noble metal particles and islands are reported by Wokaun *et al.* [2]. The synthesis and study of quantum-size effects in gold-coated nanoparticles are the subject of an article by Zhou *et al.* [3].

In this report the results will be presented of a study of the surface plasmon resonance in supported small gold and copper particles. The theory of these resonances will be discussed in chapter 2 after which ellipsometry, the experimental technique used to study this effect, is described in chapter 3. Small metal particles on a flat substrate have been prepared with the spin-coat deposition technique. With this technique it is possible to get a homogeneous, dense particle distribution over a wide range of particle sizes ranging down to as small as 1 nanometer. Determination of the particle size and distribution is

done with Atomic Force Microscopy. The deposition and characterisation of the particles are described in chapter 4. Finally the results will be discussed in chapter 5 and some recommendations for further study are given at the end of that same chapter.

Chapter 2

Optical response of metal particles

In this chapter the response of metal clusters to an applied electromagnetic field is described. After some elementary electromagnetic theory in section 2.1, absorption mechanisms are treated in section 2.2. Surface plasmons and plasmons in small metal particles are described in section 2.3 and 2.4 respectively.

2.1 Electromagnetic Theory

Macroscopically the propagation of an electromagnetic wave through a medium is described by the Maxwell equations together with constitutive relations that include the properties of the medium. Plane wave solutions of these equations for the electric field **E** are of the form

$$\mathbf{E} = \mathbf{E}_0 \exp(i\mathbf{k}\cdot\mathbf{r} - i\omega t), \tag{2.1}$$

where ω is the angular frequency, $\mathbf{r}$ is the position vector, t is the time and $\mathbf{k}$ is the wavevector. The wavevector and the angular frequency are related through the dispersion relation

$$\mathbf{k}\cdot\mathbf{k} = \omega^2 \tilde{\epsilon}\mu, \tag{2.2}$$

where μ is the *permeability* and $\tilde{\epsilon}$ the *complex permittivity.* Assumed is that the medium is isotropic, linear and homogeneous. Only non-magnetic materials are considered so that μ equals the permeability of the vacuum μ_0. Often the complex permittivity (or complex dielectric function) is given by

$$\tilde{\epsilon} = \epsilon + i\frac{\sigma}{\omega} \equiv \epsilon_1 + i\epsilon_2, \tag{2.3}$$

where ϵ is the permittivity occuring in the Maxwell equations and σ is the conductivity of the medium. The dielectric function (the addition complex is omitted from now on) is related to the complex refractive index $\tilde{n}$ through

$$\tilde{\epsilon} = \tilde{n}^2/\epsilon_0 = (n + ik)^2/\epsilon_0, \tag{2.4}$$

where n is the refractive index and k is the extinction coefficient.

Some unit systems are chosen such that ϵ_0 is dimensionless and equal to 1. This is for example the case in the Gaussian unit system. Dielectric functions are then dimensionless numbers, ususally of the order of unity. In the SI-unit system used here, one often uses a *relative* dielectric function defined as ϵ/ϵ_0. In the remaining sections of this chapter the relative dielectric function will be used without further notice, except for ϵ_0 which remains the dielectric constant in vacuum ($8.8542 \times 10^{-12} C/Vm$).

The choice in equation (2.1) to describe the electric field with a time dependence $\exp(-i\omega t)$ is completely arbitray, and could as well have been $\exp(i\omega t)$. However, the former one is the one found in standard books on optics and electromagnetic theory [4,5,8]. This sign convention makes no difference for the physics described, but care must be taken when comparing scientific literature, because it does make a difference to formulas. The dielectric function is a good example of this. In the convention used here, the imaginary part of the dielectric function is always positive. If the plus sign convention had been chosen, then the imaginary part of the dielectric function would have been negative. A last remark about sign conventions concerns the definition of ϵ_2. Often $\tilde{\epsilon}$ is written as $(\epsilon_1 - i\epsilon_2)$ to get a positive ϵ_2 when the time dependence is described with a plus sign. The same is true for the complex refractive index. As is clear from these examples care has to be taken when comparing literature.

2.2 Absorption Mechanisms

In this section the classical theories of Lorentz and Drude for absorption are described. A more extensive treatment can be found in standard books on optical properties of solids and electromagnetic theory [4–6]. Lorentz considered the electrons as independent, identical isotropic harmonic oscillators, bound to the nucleus. A viscous damping term is included in the equation of motion of the electrons to provide for an energy loss mechanism. The resulting dielectric function for such a system of bound electrons is

$$\epsilon_{bound} = 1 + \frac{\omega_p^2}{\omega_0^2 - \omega^2 - i\gamma\omega}, \tag{2.5}$$

where the plasma frequency ω_p^2 is defined by

$$\omega_p^2 = \frac{Ne^2}{m\epsilon_0} \tag{2.6}$$

and N is the electron density, m the effective electron mass, and e the charge of an electron. If more than one resonance frequency (ω_0) is possible, then these are included by adding similar terms for each frequency. The bound electron term can also be described quantum-mechanically by transitions and excitations of individual electrons. The form of

the formulas does not differ much from the Lorentz equation (2.5), but the interpretation of the terms is quite different. The quantum mechanical equivalent of (2.5) is given by

$$\epsilon_{bound} = 1 + \sum_{ij} \frac{\omega_p^2 f_{ij}}{\omega_{ij}^2 - \omega^2 - i\gamma_{ij}\omega}, \tag{2.7}$$

where the resonance frequencies ω_{ij} are now the energies (divided by $\hbar$) between the initial states (i) and the possible final states (j). The oscillator strength f_{ij} represents the probability of an excitation from an initial state i to a final state j. The damping factor γ_{ij} relates to the probabilities of transitions to all other quantum states.

However, in a free-electron material the electrons are not bound, but form a free-electron gas upon which no restoring force acts. This model, described by Drude can be obtained from the Lorentz model by omitting the restoring force term (ω_0). The dielectric function for such free electrons is then given by

$$\epsilon_{free} = 1 - \frac{\omega_p^2}{\omega^2 + i\gamma\omega} = \left(1 - \frac{\omega_p^2}{\omega^2 + \gamma^2}\right) + i\left(\frac{\omega_p^2\gamma}{\omega(\omega^2 + \gamma^2)}\right), \tag{2.8}$$

where ω_p is still given by (2.6), but now with N being the density of the *free* electrons and m the effective mass of the *free* electrons.

The term *plasma frequency* refers to the longitudinal oscillations called plasma oscillations, that occur when an electromagnetic field is applied with a frequency such that $\epsilon = 0$. When no damping is included ($\gamma = 0$), this occurs for a frequency $\omega = \omega_p$. Plasma oscillations originate from the long-range correlation of the electrons caused by Coulomb forces. In terms of quantum mechanics, plasma oscillations are quantised with the *plasmon* as the quantum of the plasma oscillation. Such a plasmon describes not one electron, but an excited state of a collection of electrons.

In a more general and realistic case, the damping is non-zero and the Drude dielectric function vanishes for the complex frequency $\omega_p - i\gamma/2$. The damping constant γ is related to the average time τ between collisions by $\gamma = 1/\tau$. Plasma frequencies for metals are in the visible and ultraviolet, with photon energies in the range from about 3 to 20 eV and for most metals at room temperature, γ is much less than ω_p. Therefore, a good approximation to the Drude dielectric function at visible and ultraviolet frequencies is

$$\epsilon_1 \simeq -\frac{\omega_p^2}{\omega^2}, \tag{2.9a}$$

$$\epsilon_2 \simeq \frac{\omega_p^2\gamma}{\omega^3}, \tag{2.9b}$$

for $\omega \gg \gamma$. Often ϵ_2 is even put equal to zero.

For most real metals Drude theory is not good enough in the range of ultraviolet and visible frequencies. Beside the free electrons, bound electrons are also present and will influence the optical behaviour. The dielectric function is then the sum of a free electron term (ϵ_f), described by Drudes theory, and a bound-electron term (ϵ_b), described by Lorentz theory. The effect of the bound electrons on the plasma frequency can be quite significant. For silver for instance, the effect of the bound electrons is that the plasma frequency shifts from 9.05 eV to 3.78 eV [7].

2.3 Surface Plasmons

As shown in the previous section, electron oscillations in the form of longitudinal waves can occur in the bulk of a metal when the dielectric function vanishes. At the surface of a metal similar oscillations can occur, which are called *surface plasmons* as opposed to the bulk plasmons. A surface plasmon is a self-sustaining oscillation of the electron gas at the surface characterised by an exponential decay of the potential Φ associated to it, both toward the vacuum and toward the bulk, and by an oscillatory behavior along the surface [7]. The potential Φ can be described by:

$$\Phi(\mathbf{r}) = \Phi_0 \exp(i\mathbf{q}_{\|}\cdot\mathbf{r}_{\|}) \exp(-q_{\|}|z|), \tag{2.10}$$

where $\mathbf{r}_{\|}$ defines the position vector in the plane, $\mathbf{q}_{\|}$ is the momentum of the surface plasmon and z the distance normal to the surface from the truncation plane of the crystal, half a lattice spacing away from the outermost ion cores. For a metal, the z component of the electric displacement vector $\mathbf{D} = \epsilon\mathbf{E}$ must be continuous across the metal/ambient interface. With $\mathbf{E}$ derived from the potential Φ and a surface plasmon frequency ω_{sp}, this can only be satisfied if

$$\epsilon(\omega_{sp}) = -\epsilon_a, \tag{2.11}$$

where ϵ and ϵ_a are the dielectric function of the metal and the ambient respectively. For the metal/vacuum interface this means that $\epsilon(\omega_{sp}) = -1$. For a free-electron metal, using equation (2.9) and assuming ϵ_2 to be negligible, this results in a surface plasmon frequency ω_{sp} given by

$$\omega_{sp} = \omega_p\sqrt{2}. \tag{2.12}$$

The presence of d-bands and the d→s interband transitions in noble metals and d-metals in general, displaces the plasma and surface plasmon peaks considerably with respect to the values appropriate for a free-electron metal. The dielectric function now has a bound (ϵ_b) and a free-electron (ϵ_f) term and a surface plasma resonances is expected when $\epsilon(\omega_{sp}) = \epsilon_b(\omega_{sp}) + \epsilon_f(\omega_{sp}) = -\epsilon_a$.

2.4 Metal Particles

Surface modes are also possible for small spherical particles. The condition that has to be satisfied is now

$$\epsilon = -2\epsilon_a, \tag{2.13}$$

where ϵ_a is the dielectric function of the surrounding medium [8]. The frequency at which this condition is satisfied is known as the Mie frequency ω_M. If $\gamma \ll \omega_p$, it follows from (2.9) that

$$\omega_M = \frac{\omega_p}{\sqrt{1+2\epsilon_a}} \tag{2.14}$$

for a spherical free-electron metal particle, which reduces to $\omega_M = \omega_p/\sqrt{3}$ if the particle is in vacuum or air where $\epsilon_a = 1$.

One way of dealing with the cluster-size dependence of ω_M is through the mean free path of the electrons. Due to the size of the particles, the mean free path of the free electrons is drastically decreased in comparison with a flat surface. As a consequence, the damping constant γ in the Drude theory is increased and γ can be written as

$$\gamma = \gamma_{bulk} + \frac{v_F}{L}, \tag{2.15}$$

where γ_{bulk} is the bulk metal damping constant, v_F is the electron velocity at the Fermi surface, and L is the effective mean free path. The result is that the Mie frequency will shift towards the *red* (lower frequency) with a *decreasing* particle diameter. This is an effect confirmed experimentally for simple metals like sodium and potassium [9] as long as the particle diameter is not too small.

Another way of explaining the Mie resonance shift in particles is by the use of the dynamic screening theory. As an external electromagnetic field is applied to the metal surface, a surface charge density will be induced. This induced charge screens the rest of the metal from the applied electromagnetic field. The induced charge is partly "spilled out" into the vacuum reducing its binding and thus also decreasing the resonance frequency. The amount of "spill out" depends on the particle size and on the localisation of the electrons. The *sp*-electrons that form the induced surface charge, are only weakly localised for very large particles, but will be more localised when the particles get smaller. At a certain particle size the effect of the localisation will be stronger than the effect of induction of surface charge by the applied field. A more localised electron also means that the binding is stronger and thus will the resonance frequency shift to higher frequencies. This effect of a red shift with decreasing particle size until a certain particle size and then a blue shift if the particle size is even more decreased, has been observed experimentally by Reiners *et al.* [9] for sodium.

Further decrease of the particle size will eventually result in the disappearence of the Mie resonance as the *sp*-bands will break up into separate electron states. A collective oscillation of the electrons is then not possible anymore.

However, for metals with *d*-electrons as for instance silver and gold, only a blue shift is observed [10–12]. It is assumed that the *sp*-electrons are already weakly localised due to the presence of the *d*-electrons. The interaction between *d*- and *sp*-electrons is very subtle and cannot be treated in a general way. One can only say that due to this interaction, the *sp*-electrons will have a stronger binding and thus also a higher resonance frequency.

For a more quantitative description of the shift of the resonance frequency, the dielectric function of the particles is slightly modified. Here the model used by Kreibig *et al.* [13] is given. The dielectric function is again written as a sum of a free electron term and a bound-electron term:

$$\epsilon = 1 + \frac{\omega_p^2}{\omega_0^2 - \omega^2 - i\gamma\omega} + \epsilon_{ib}. \tag{2.16}$$

The free-electron term is actually written as a Lorentz term, but with the resonance frequency ω_0 depending on the size of the particle via

$$\omega_0 = 1.3 v_F / R, \tag{2.17}$$

where v_F is the Fermi velocity and R the radius of the particle [3, 13]. The damping γ is again given by (2.15) and the contributions of interband transitions are in (ϵ_{ib}) for which the bulk value is used. For very large particles ω_0 is negligible and the free electron term reduces to a Drude term. The damping term $i\gamma\omega$ broadens the resonance peak for decreasing particle size, something which is clearly observed in for instance Electron Energy Loss Spectroscopy (EELS) on gold clusters [14]. With equation (2.17), decrease of the particle diameter will increase the resonance frequency ω_0. Using this with (2.16) in the resonance condition (2.13), one can see that the Mie resonance frequency will also shift to higher frequencies when the particle diameter decreases.

Chapter 3
Ellipsometry

Upon reflection from a surface, the polarisation state of a polarised light beam will change. The branch of optical spectroscopy which measures the changes in the polarisation state is called ellipsometry.

The polarisation state of a light beam is defined by two parameters, i.e. the relative phase and the amplitude of the orthogonal electric field components. Thus in an ellipsometry experiment it is possible to determine *two* independent parameters: the change in relative phase and the change in amplitude of these two electric field components. The measurements can be related to physical properties of the material being studied with appropriate models. These properties are for example the real and imaginary part of the complex dielectric function ($\tilde{\epsilon} = \epsilon_1 + i\epsilon_2$) of a bare reflecting surface or the thickness and the refractive index of a transparant film on a known substrate.

Like most optical spectroscopies, ellipsometry has the advantage of being non-destructive, doesn't require ultra high vacuum systems like electron spectroscopies and thus also makes it possible to do *in situ* measurements during, for example, the growth process. Compared to other optical spectroscopies, ellipsometry has the advantage of being very sensitive to small changes at the surface. As a phase measuring technique it is unaffected by intensity fluctuations and has a high precision compared to intensity measurements.

In the next section the general principles of ellipsometry will be discussed, after which some simple models are treated in section 3.2. The enhancement of the sensitivity for very thin films on a substrate discussed in section 3.3 is followed by a description in section 3.4 of the ellipsometer used for the experiments in this report. More extensive treatments of ellipsometry and its instrumentation can be found in references [15, 16].

3.1 General principles of ellipsometry

For the description of the interaction of electromagnetic waves at optical frequencies with nonmagnetic materials one uses the electric field. The electric field can be decomposed into components parallel, p, and perpendicular, s (from the German *senkrecht*) to the plane of incidence as shown in figure 3.1. The plane of incidence is the plane spanned by the surface normal of the sample and the wavevector of the incoming electromagnetic wave.

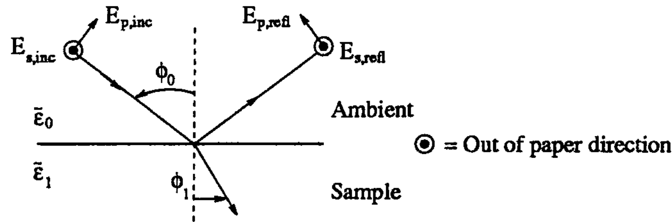

Figure 3.1: *Reflection from a sample. The complex dielectric function of the sample and the ambient are denoted by $\tilde{\epsilon}_1$ and $\tilde{\epsilon}_0$. The angles of incidence and refraction are ϕ_0 and ϕ_1 respectively.*

The change in the electric field upon reflection from an isotropic sample is described by the amplitude reflection coefficients, defined as

$$r_p = \frac{E_{p,refl}}{E_{p,inc}} \qquad \text{and} \qquad r_s = \frac{E_{s,refl}}{E_{s,inc}} \tag{3.1}$$

for p and s polarisation respectively. The polarisation state of a light beam is defined as

$$\chi = \frac{E_s}{E_p} \tag{3.2}$$

and the relative change in polarisation state upon reflection from an interface is given by the complex reflectivity ratio

$$\rho = \frac{\chi_{inc}}{\chi_{refl}} = \frac{r_p}{r_s}. \tag{3.3}$$

Usually ρ is expressed in terms of conventional ellipsometric angles Ψ and Δ which can be introduced after rewriting ρ in terms of the magnitude ($|r|$) and phase (δ) of the reflection coefficients:

$$\rho = \frac{|r_p|}{|r_s|}\exp[i(\delta_p - \delta_s)] = \tan\Psi\exp(i\Delta). \tag{3.4}$$

Ellipsometric experiments give $\tan(\Psi)$ and $\cos(\Delta)$, which can be interpreted in terms of sample properties. Some simple models will be treated in the next section, where the relation is studied between the dielectric function of the materials studied and ρ. The microscopic interpretation of the dielectric function has been described in chapter 2.

3.2 Simple models

The simplest model is the *two phase* model, where the two phases refer to a semi-infinite sample and the ambient. This model is often used for bulk materials. By matching the

electric and magnetic field components at the surface one obtains the well known Fresnel equations for optically isotropic materials (see for example [17])

$$r_p = \frac{\sqrt{\tilde{\epsilon}_0}\cos\phi_0 - \sqrt{\tilde{\epsilon}_1}\cos\phi_1}{\sqrt{\tilde{\epsilon}_0}\cos\phi_0 + \sqrt{\tilde{\epsilon}_1}\cos\phi_1} \tag{3.5a}$$

and

$$r_s = \frac{\sqrt{\tilde{\epsilon}_1}\cos\phi_0 - \sqrt{\tilde{\epsilon}_0}\cos\phi_1}{\sqrt{\tilde{\epsilon}_1}\cos\phi_0 + \sqrt{\tilde{\epsilon}_0}\cos\phi_1}, \tag{3.5b}$$

expressing the amplitude reflection coefficients of an interface in terms of the angles of incidence and refraction (ϕ_0, ϕ_1) and the complex dielectric functions of the two media $(\tilde{\epsilon}_1, \tilde{\epsilon}_0)$ as defined in figure 3.1. From these equations and the definition of ρ (eq. 3.3) one can get a relation, directly expressing the complex dielectric function $\tilde{\epsilon}_1$ of the sample in terms of ρ and the incidence angle:

$$\tilde{\epsilon}_1 = \tilde{\epsilon}_0 \sin^2\phi_0 \left[1 + \left(\frac{1-\rho}{1+\rho}\right)^2 \tan^2\phi_0\right]. \tag{3.6}$$

This relation is only valid for ideal surfaces with properties that do not differ from the bulk of the sample. Applied to real samples, the resulting dielectric function is referred to as the pseudo-dielectric function. The non-ideal surface layer can also be considered as a seperate layer, in which case the sample is described with the *three phase* model.

The propagation of light in a three phase system is schematically shown in figure 3.2. For thin or transparent overlayers, multiple reflections in the overlayer have to be taken into account. The total reflection coefficient for α-polarised (α=s or p) light for the three

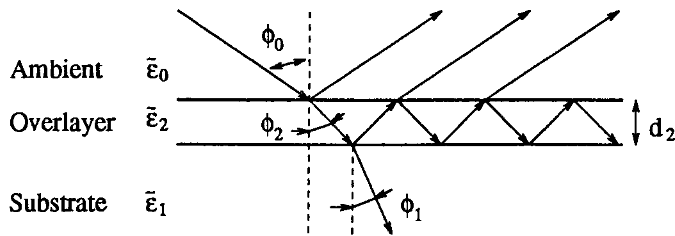

Figure 3.2: *Propagation of light in a three phase system. The complex dielectric functions of the three phases are $\tilde{\epsilon}_1, \tilde{\epsilon}_0$ and $\tilde{\epsilon}_2$ respectively. The overlayer has a thickness d_2.*

phase system is

$$r_\alpha = \frac{r_{02}^\alpha + r_{21}^\alpha X}{1 + r_{02}^\alpha r_{21}^\alpha X}, \tag{3.7a}$$

where r^{α}_{lm} is the Fresnel coefficient for α-polarised light at the interface between the media l and m and

$$X = \exp[\frac{-4\pi i d_2 n_2 \cos\phi_2}{\lambda}]. \tag{3.7b}$$

The thickness of the overlayer is d_2, λ is the wavelength of the light in vacuum, ϕ_2 the angle of refraction in the overlayer and n_2 the complex refractive index[1] of the overlayer. Extension of such modelling to more layers is straightforward and is most easily done in terms of the *optical impedance* of a layer.

3.2.1 Impedance formalism

The advantage of the impedance formalism is that the equations for s and p polarisation have the same appearance, with the difference being in the impedance factors itself. The impedance factors f_{pl} and f_{sl} of an isotropic medium l are defined as (see for example [18,19])

$$f_{pl} := \frac{\cos\phi_l}{n_l} = \frac{\sqrt{n_l^2 - n_0^2 \sin^2\phi_0}}{n_l^2} \tag{3.8a}$$

$$f_{sl} := n_l \cos\phi_l = \sqrt{n_l^2 - n_0^2 \sin^2\phi_0}, \tag{3.8b}$$

where Snell's law and basic trigonometry have been used to eliminate ϕ_l from the expressions. The subscript 0 denotes the medium through which the light originally propagates (the ambient, usually being air, vacuum or in the case of plasma deposition, the plasma) and does not necessarily have a direct boundary with the medium l. The indices of refraction n_l as well as the angles with the surface normal ϕ_l are in general complex quantities.

With equation (3.8), equation (3.5) for the reflectivity coefficients of α polarised light can be rewritten as

$$r_{\alpha lm} = \frac{f_{\alpha l} - f_{\alpha m}}{f_{\alpha l} + f_{\alpha m}}, \tag{3.9}$$

where l is the incident medium and m the refractive medium. The subscripts indicating the polarisation will be omitted from now on as it makes no difference to the form of the equations.

The total amplitude reflection coefficient for a substrate with k layers on top is now determined in an iterative process. The reflection coefficient of the substrate plus the first layer is calculated and from this an effective optical impedance for the effective substrate (substrate plus first layer) is determined. In the next step the procedure is repeated for the second layer on the effective substrate. This procedure is repeated until the system is

[1] In SI-units, the complex refractive index of a non-magnetic material is related to the complex dielectric constant by $n^2 = \tilde{\epsilon}/\epsilon_0$, where ϵ_0 is the dielectric constant of the vacuum.

reduced to a system with one layer, that being the kth layer in the original model, and an effective substrate made up of the real substrate plus $(k-1)$ layers.

As an illustration the effective optical impedance of a substrate plus one layer is now derived. The amplitude reflection coefficient for a substrate plus one layer (equation (3.7)) can be written as

$$r = \frac{r_{02} + u}{1 + r_{02} u} \tag{3.10a}$$

with

$$u = r_{21} \exp(-2i\beta_2) \tag{3.10b}$$

and

$$\beta_l = \frac{2\pi d_l n_l \cos\phi_l}{\lambda} = \frac{f_{sl} 2\pi d_l}{\lambda} \tag{3.10c}$$

and the media 0, 1 and 2 are the ambient, substrate and first layer respectively. The next step is to treat the substrate plus film together as the effective substrate for the next layer. This new substrate will be called medium x with one effective impedance f_x that can be determined from equations (3.9) and (3.10) leading to the equation

$$r_{0x} \equiv \frac{f_0 - f_x}{f_0 + f_x} = \frac{r_{02} + u}{1 + r_{02} u}. \tag{3.11}$$

Solving this equation for f_x leads to

$$f_x = f_2 \frac{1 - u}{1 + u}. \tag{3.12}$$

With this effective impedance of the substrate plus first layer and the impedance of the second layer the amplitude reflection coefficients can be calculated for the substrate plus two layers. For every next layer the whole procedure is repeated.

3.3 Enhanced surface and interface sensitivity

Ellipsometry directly gives information about a layer on a substrate even if this layer is very thin. However, for some materials the difference between the properties of the layer and the bulk is very small, making it hard to detect this layer. The detection of thin layers at the vacuum-substrate interface can be enhanced by choosing a multilayer substrate in such a way that there is an (nearly) anti-reflection condition for the s polarised light. In figure 3.3 such a sample is shown schematically. This technique was first described by Theeten *et al.* [20] for the study of the interface between GaAs and its plasma-grown oxide and later also used by Jans and Gemmink [21] for the detection of very thin *a*-Si:H coatings on oxidized *c*-Si.

At the wavelengths used, the SiO_2 layer is transparent and multiple reflections in the SiO_2 layer will give rise to interference effects resulting in an anti-reflection condition for

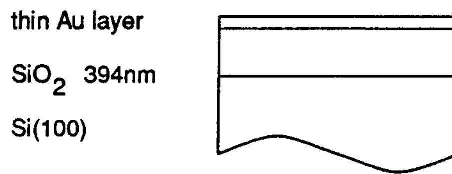

Figure 3.3: *Schematic representation of a sample used for resonant spectroscopic ellipsometry. The SiO_2 layer is artificially grown with such a thickness that resonances will occur at specific wavelengths.*

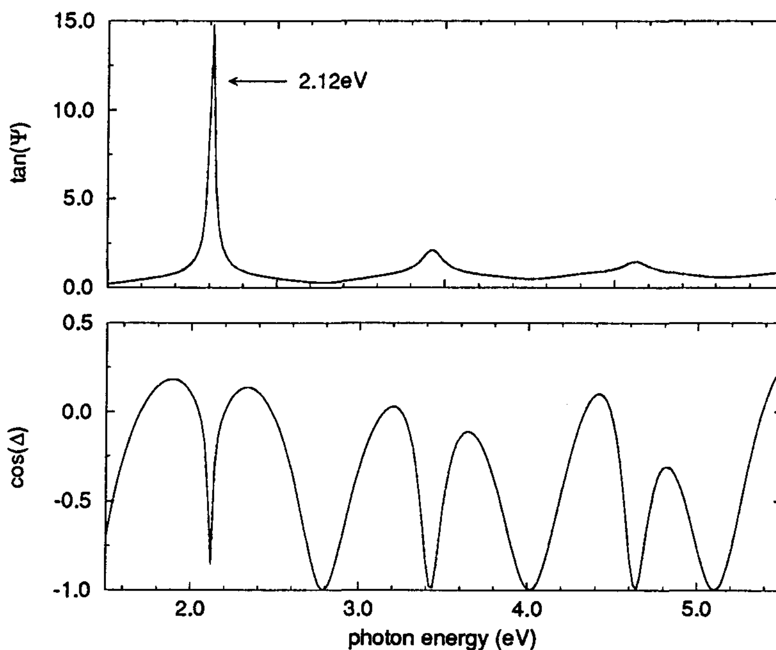

Figure 3.4: *Simulated ellipsometry spectrum of silicon with a 394 nm SiO_2layer. Equation 3.7 is used with an incidence angle of 70° and values for the complex refractive index of c-Si and SiO_2 from Palik [22].*

the s component of the electric field at certain wavelengths. In the case where r_s (nearly) equals zero $r_p \gg r_s$ and as a consequence $\tan(\Psi) = |\rho| \rightarrow \infty$, while the phase ($\Delta$) goes to 180° as can be seen in figure 3.4. The first resonance occurs here at a photon energy of 2.12 eV. The anti-reflection situation depends strongly on the surface. The presence of a very thin layer can be seen as a shift of the resonance position and a decrease of $\tan(\Psi)$ at resonance. The dip in $\cos(\Delta)$ at resonance also changes in a peak. Because of experimental errors, it is better for very thin layers not to look at the change in $\tan(\Psi)$ at resonance,

but just at the change in $\cos(\Delta)$.

3.4 Instrumentation

3.4.1 Ellipsometers in general

As mentioned in the introduction, ellipsometry measures the change in the polarisation state of a beam of light upon reflection from a sample. The main components of an ellipsometer are a light source and polariser, producing a linearly polarised beam of light which impinges on the sample, a second polariser acting as analyser and a detector to analyse the polarisation state of the reflected beam. A compensator, introducing a phase shift between the two polarisation states, can be inserted either between the sample and the analyser or between the polariser and the sample if required. A schematic representation of such a setup is shown in figure 3.5.

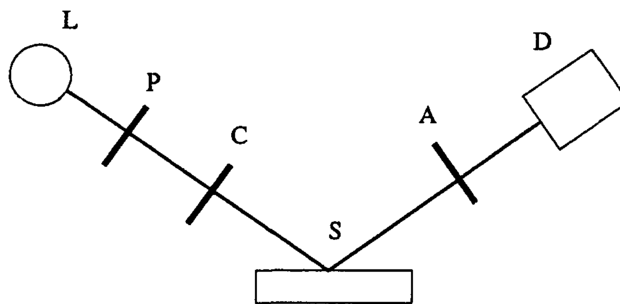

Figure 3.5: *General setup of a PCSA ellipsometer. The function of the components is described in the text. L: light source, P: polariser, C: compensator, S: sample, A: analyser, D: detector.*

With *null-ellipsometry* the ellipsometer settings are tuned to reduce the intensity, measured at the detector, to zero. This is a time consuming method which makes it impossible to monitor fast processes, such as layer growth. It also requires that the experiment is done at a single wavelength at a time so that a monochromator has to be inserted between light source and polariser.

In photometric experiments one of the ellipsometer settings is modulated with time and the detector response is recorded as a function of time. Fast analysis of this response makes it possible to do real-time measurements of fast processes.

Hereafter the *rotating analyser ellipsometer* will be described in more detail, as this is the one used for the results described in this work. Other photometric ellipsometers have as time modulated components either a rotating compensator, a photo-elastic modulated compensator or a rotating polariser.

3.4.2 Ellipsometer at the Philips Research Laboratories

The ellipsometer used for the experiments is a spectroscopic rotating analyser ellipsometer designed and build at the Philips Research Laboratories Eindhoven[2] (PRLE). This ellipsometer has been described by Jans [23] and is of the same type as the one described by Aspnes and Studna [24]. A schematic representation of the ellipsometer is given in fig-

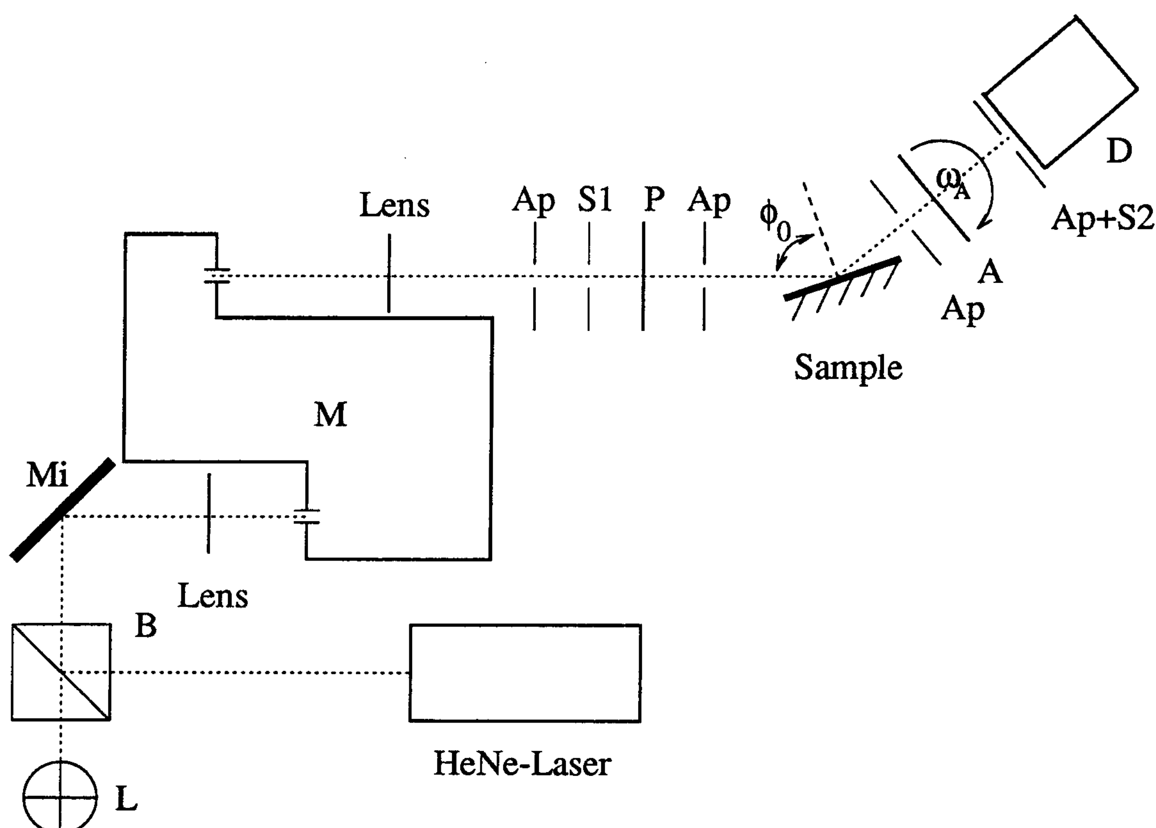

Figure 3.6: *Schematic representation of the ellipsometer used for the experiments. A description of the components is given in the text.*

ure 3.6. In this setup the lightsource (L) is a 75-W Xe high-pressure arc lamp and the monochromator (M) is a Cary 14 fore-prism grating double monochromator. With this monochromator, scans over a wide range of frequencies are possible without changing the filters. A second order spectrum is prevented by the fore-prism. The detector (D) is an EMI 9558QB(S20)-tube photomultiplier and the polarisers (P and A) are Glan-type calcite polarising prisms. The analyser prism (A) rotates with an angular frequency ω_A. The beam is collimated with lenses and apertures (Ap). The shutter S1 is closed for background measurements and the shutter S2 is used to protect the photomultiplier tube. For alignment

[2]Philips Research Laboratories Eindhoven, P.O. Box 80000, 5600 JA Eindhoven, The Netherlands

purposes a He-Ne laser is used. The laser beam is coupled into the system by a beamsplitter (B), which is removed from the lightsource beam during experiments. Monochromator, angle of incidence (ϕ_0), and polariser are stepping-motor controlled. Measurements are done in the photon energy range from 1.6 up to 5.4 eV at an incidence angle of 70 degrees. A polariser angle of 20 degrees with respect to the plane of incidence is used. Averaging of the spectra taken at plus and minus 20 degrees eliminates first order errors arising from misalignment. The whole setup is in air in a darkroom. Control of the measurement and data-acquisition is done by a computer with an OS-9, multi-user operating system and custom designed software. Additional software on the OS-9 system, developed at the PRLE is used for data analysis. A commercial software package *V.A.S.E.* [25] running under the MS-Windows^{tm} system on a personal computer, is also available for data analysis.

The detected signal as a function of analyser angle $A = \omega_A t$ is given by

$$I_d = g(1 + a\cos 2A + b\sin 2A), \tag{3.13}$$

where the coefficients a, b and g are determined by Fourier analysis of the signal. The coefficients a and b may be expressed in terms of the polariser angle (P) and the sample characteristic angles Ψ and Δ by

$$a = \frac{\cos 2P - \cos 2\Psi}{1 - \cos 2P \cos 2\Psi} \tag{3.14a}$$

and

$$b = \frac{\sin 2P \sin 2\Psi \cos\Delta}{1 - \cos 2P \cos 2\Psi}. \tag{3.14b}$$

In these equations the angles A and P are relative to the plane of incidence which is in general not the same as the position of the component relative to its own coordinate system, indicated by A' and P'.

Calibration is necessary to establish the exact position of the plane of incidence and to correct for the additional phase shift and amplification factor in the detected signal induced by the electronics in the detection circuit. The detected intensity can be rewritten as

$$I_d = g'(1 + \sqrt{a'^2 + b'^2}\cos(2A' + \phi')), \qquad \text{where} \qquad \phi' = \arctan\left(\frac{b'}{a'}\right), \tag{3.15}$$

where the primed quantities denote the actual measured values with respect to the coordinate system of the components. This should be identical to the ideal situation as in equation (3.13). The residue calibration procedure uses the equality of the prefactors $\sqrt{a^2 + b^2}$ and its primed equivalent, while equality of the arguments leads to the phase calibration procedure [16, 18, 19, 26]. Residu calibration is preferable for samples with Ψ and Δ close to 45° and 90° respectively, whereas the phase calibration works better for Ψ close to 0° or 90° and for Δ close to 0° or 180°.

In the experiments described in this report, residu calibration is used. The photon energy at which the calibration is done is chosen in such a way that the aforementioned preferred values for Ψ and Δ are attained. This means that for silicon, with a native oxide layer, the calibration was done at a photon energy of 4.0 eV, while for silicon with a 394nm oxide layer a photon energy of 1.6 eV was chosen.

Chapter 4

Supported metal particles: preparation and characterisation

Studies of optical and electronic properties of small metal particles can be caried out, for example, on particles embedded in a transparent matrix (e.g. glass or condensed Ar) or on particles supported by a (flat) dielectric substrate (e.g. quartz or SiO_2/Si). For the study of size dependent effects in metal particles, control of the size and distribution of the particles is very important. In the last two years the technique of spin-coating for the preparation of metal particles on flat supports [27–29], has generated considerable interest. This technique will be described in the next section. Characterisation of the particle size and distribution will be discussed in section 4.2.

4.1 Preparation of nanometer-sized metal particles

In catalysis research, model systems of small metal particles on a flat substrate have been studied extensively. These particles can be prepared in different ways. The first method follows the steps used in industry, where after deposition and distribution of the precursor compound on the support, the sample is dried and possibly calcined leading to the formation of the metal oxide state. To obtain the metalic state of the particles the precursor compound or metal oxide is then reduced. Deposition and distribution is done by adsorption or impregnation, depending on whether or not there is interaction with the support.

Evaporation of the metal in an ultra high vacuum (UHV) system is another deposition technique. The evaporated metal will be deposited on the substrate and small particles may be formed. With this method it is possible to grow small particles, islands and even complete layers of the metal. Similar to this method is sputter deposition, where a metal target, placed in close proximity of the substrate, is bombarded with high-energy ions. Metal atoms will be sputtered from the target and deposited on the substrate.

Recently the technique of spin-coating has been introduced to deposit small metal particles on flat substrates. This technique is widely applied in industry, for instance for the deposition of photo-resist films, but it was only recently that Kuipers *et al.* [30] introduced this technique in catalysis for the deposition of metal particles on flat substrates. Spin-coating allows for a controlled particle size with a narrow distribution window. Furthermore

is it possible to get a homogeneous, dense particle distribution over a wide range of particle sizes ranging down to as small as 1 nanometer.

For the deposition of metal particles a precursor containing the metal (e.g. a metal salt) is dissolved in a highly volatile solvent. This solution is deposited onto a flat substrate which is simultaneously, or subsequently, spun at a high rotational frequency. The centrifugal forces cause the solution to spread and the solution will form a uniform film on the substrate, while residual material is ejected from the substrate. Due to evaporation of the solvent, the solution will become supersaturated and metal particles will form and deposit onto the substrate.

Among the experimental factors that influence the size and distribution of the particles are the initial solute concentration of the solution, the viscosity and evaporation rate of the solvent, and the spin frequency. Another important factor is the atmosphere in which the spin coating is done, e.g. through its influence on the evaporation rate and through the influence of its humidity on the homogeneity of the particle distribution. Water, either condensed from the air or present in the solvent, can break up the film causing areas without particles and an increased particle density at the border of these areas. By using an inert atmosphere like nitrogen or argon and very pure solvents and solutes this problem is minimised. In solutions which have been allowed to stand for a relatively long period of time, precursor material tends to agglomerate. Poor control of the particle size and an inhomogeneous deposition will result. To prevent this, fresh solutions should always be used.

After the spin-coating, the samples undergo heat treatments to form the actual metal particles. Heating in air (calcination) or oxygen (oxidation), can decompose the metal precursor and subsequently oxidise the metal compound. Care must be taken with temperature control, since too high a temperature may induce a redistribution of the metal particles leading to either sintering of the deposited material or, alternatively, breaking up of the particle into even smaller particles. Some species, such as carbon impurities, are also removed from the surface by calcination. This is important since they can seriously affect the surface sensitive techniques used in analysis of the samples.

The sample is reduced to transform the formed metal oxide, or the precursor compound into metal particles. This means that it is heated in a reducing atmosphere such as hydrogen. The reduction not only transforms the particles into the metallic state, but also causes a particle-substrate interaction that is strong enough to prevent the particles from being removed from the substrate by an AFM tip during experiments [27]. As with calcination high temperatures may cause sintering or breaking up of the formed particles.

For calcination as well as reduction, conditions such as heating rate, final temperature, duration of the heat treatment and gas pressure affect the final distribution of the particles. The effects of these parameters as well as spin-coat parameters like initial solute concentration, solvent, and rotation speed have been studied by for example Partridge *et al.*, Kuipers *et al.* and Doornkamp *et al.* [27,28,30].

4.1.1 The spin-coat facility

A simple self-built spin-coat facility present in the Surface and Interface Physics group [29] has been used for the deposition of the metal particles onto flat supports. A laboratory centrifuge (type HEKA) with an aluminum platform mounted on the motor axis as sample support was used to spin the samples. Rotational frequencies from 735 up to 10,000 rpm are possible by applying different motor voltages subject to calibration. The spin-coater is placed inside a glove-box with a load-lock. Water absorbing crystallites (like $Cu(NO_3)_2$) and zeolites are used to maintain a low (<20%) humidity inside the glove-box. The glove-box can also be purged with inert gas (e.g. Ar or N_2) to decrease the relative humidity and enhance the evaporation of the solvents.

4.2 Sample Characterisation

Several experimental techniques have been used to characterise the deposited particles before, or when necessary after, the ellipsometry experiments. A rough indication of the homogeneity of the particle distribution was obtained with optical microscopy, while more detailed information was obtained with scanning electron microscopy (SEM). Determination of particle size and distribution was done with atomic force microscopy (AFM). In the next two sections AFM and SEM are briefly discussed. The discussion of the AFM will be more involved as this is the most important technique used here for determination of size and distribution of (very small) particles.

4.2.1 Atomic Force Microscopy

During the last decade a completely new type of microscopy has been developed. The generic term for these techniques is Scanning Probe Microscopy (SPM). The sample surface is scanned by a mechanical point probe by means of piezo electric transducers, very close to the surface. The probe senses the surface by some kind of interaction and a feedback signal is provided. An image of the specific surface-probe interaction is obtained by monitoring this feedback signal. The advantage of SPM is that a much higher magnification is possible than with conventional microscopies, even down to atomic resolution.

The first type of SPM developed was Scanning Tunnelling Microscopy (STM) in 1982 by Binning and Rohrer. In STM, a sharp tip is placed within a few Ångstroms of the surface of a conducting sample. Due to the overlap of the electronic wave functions in the tip and the surface, it is possible for electrons to tunnel between the tip and the surface when a voltage is applied between the tip and the surface. This tunnel current provides an image arising from the convolution of the electronic states of the tip and the surface. A high spatial resolution ($\sim$1Å laterally and $\sim$0.01Å vertically) can be achieved. Its main disadvantage however, is the restriction to conducting samples.

New SPM techniques, depending on other probe-surface interactions, have been developed. For probing magnetic properties of surfaces for example, Magnetic Force Microscopy was developed. The most widely applied SPM technique however, is AFM. Here a sharp

probe tip mounted on a flexible cantilever is scanned across the sample. The distance between tip and surface atoms is in the (sub)nanometer range. Due to the interaction between tip and surface atoms, the cantilever will deflect. This deflection is optically monitored and feedback signals are generated. From the deflection as function of the lateral displacement a three-dimensional image of the surface is generated.

A variety of different forces are responsible for the surface-tip interaction. Among these forces are:

- Van der Waals forces
- ionic repulsion
- electrostatic forces
- magnetic forces
- frictional and adhesion forces

A simple model for the tip-sample interaction can be described by combining the attractive Van der Waals and the repulsive electron interaction potentials in the so called Lennard-Jones interaction potential:

$$E = 4\varepsilon\left(\left(\frac{\sigma}{r}\right)^{12} - \left(\frac{\sigma}{r}\right)^{6}\right), \tag{4.1}$$

where ε and σ are constants and r represents the distance between the interacting atoms.

An AFM can be operated in several modes depending on tip-sample distance and the way the cantilever is manipulated.

In the *non-contact mode* the average tip-sample distance is of the order of several nanometers. The interactions in this mode occur between many atoms which leads to a limited lateral resolution. Information about the surface structure is obtained in this mode and with the interaction forces being in the picoNewton range, it is ideal for monitoring surfaces highly sensitive to deformation. Often a dynamic measuring method is applied, predominantly to increase the sensitivity to the interaction force. In this method the cantilever is forced to vibrate at a high frequency by a piezoelectric element. The gradient of the interaction force will cause a change in the resonance frequency of the cantilever, leading to a perturbation in the vibration amplitude or phase, which is detected. This is the so-called tapping mode.

In the *contact mode* the sample-tip distance is of atomic dimensions, usually a few Ångstroms. A high lateral and vertical resolution is achieved, because the sample-tip interaction is generally determined by the interaction between individual atoms at the apex of the tip and their nearest neighbour atoms on the sample. Care has to be taken that the sample is not deformed, since the interaction forces are relatively high (in the order of nanoNewton). Two methods can be used when measuring in contact mode. The first

one is the *constant force mode* in which the force between tip and sample is kept constant. This requires an accurate feedback signal and makes these measurements relatively slow. In this mode the feedback is used to make an image of the surface.

The second method is the *variable lever deflection mode*, in which the image is immediatly obtained from the deflection of the cantilever. Although faster, this mode has the disadvantage that the tip can crash into steep sided surface objects, since there is no accurate feedback system.

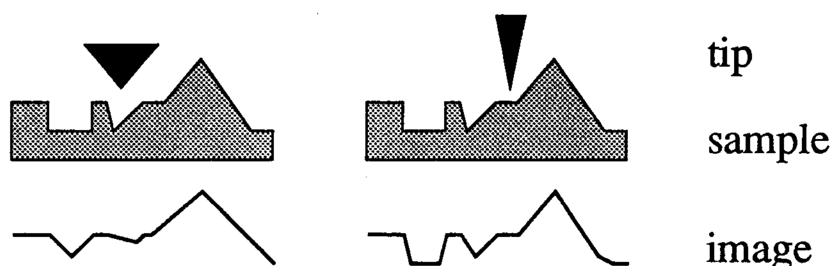

Figure 4.1: *Effect of the tip shape on the AFM image for a blunt and a sharp tip.*

Interpretation of SPM images is not trivial. The images obtained involve the convolution of tip and surface structure. As illustrated in figure 4.1 for AFM, blunt tips will provide lower contrast information and can even exhibit more characteristics of the tip shape rather than the topography. Multiple tip interactions are another source of image distortion.

The AFM in the Surface and Interface Physics group is an Omicron AFM, situated in a small chamber connected directly to an UHV system [29]. This AFM uses the optical deflection detection method. In this method a small intense infra-red light-beam is focussed on the backside of the cantilever. The reflected light is detected by a position-sensitive diode, consisting of a four quadrant photosensitive array. This enables the simultaneous measurement of both topography and friction. In the constant force mode, the feedback voltage of the z-piezo is digitised and displayed as a topological profile of the surface. Scans of the surface can be carried out in a frame of 5×5 μm with a maximum vertical displacement of 280 nm.

4.2.2 Electron Microscopy

In electron microscopy the sample is scanned with a focussed beam of high energy electrons (typically 5-30 keV). Several interactions occur and a variety of signals can be detected. Information about surface morphology, crystallography and chemical composition can be obtained by use of the appropriate detectors.

In scanning electron microscopy (SEM) the secondary and backscattered electrons are detected. The secondary electrons have a low energy (10 to 50 eV) and give information

from the surface layer only, with a maximum resolution of several nanometers. Backscattered electrons have a higher energy and penetrate the sample deeper, revealing information about the sample composition. In SEM images the heavier elements appear brighter since they scatter electrons more efficiently.

The high energy electrons ionize atoms, after which the atoms emit X-rays. These X-rays have an element characteristic energy dispersion. In *Energy-Dispersive X-ray Spectroscopy* (EDX) these emitted X-rays are detected and chemical information of a small selected surface area is obtained.

Chapter 5

Results

The objective of this project is the optical study of the electronic properties of very small supported metal particles and the size dependence of these properties. The main interest was in the detection of the plasma or Mie resonance in the particles as described in chapter 2. Spectroscopic ellipsometry has been used and to increase the sensitivity of the ellipsometer to small particles, they were deposited on silicon with an artificially grown oxide layer (see section 3.3).

Spin coating, as described in chapter 4, was used to deposit the particles on the substrate, while AFM was used to determine particle size and distribution.

The ellipsometer operates in the ultra-violet and visible light regime, which requires the choice of metal particles with a Mie frequency within this regime. As the deposition of ultra-small copper particles had already proven to be succesfull [27, 29, 30] and as copper is a well-studied metal, it was decided that copper particles constituted the most suitable system to study. However, in the literature, there have also been numerous reports about the properties of small metal particles, especially gold and silver [10–14, 31, 32]. Thus gold particles were also chosen for ease of comparison.

In section 5.1 the results for the gold particles will be presented and discussed, while the results for the copper particles are presented and discussed in section 5.2. Recommendations for future work are given section 5.3.

5.1 Gold particles

Large and small gold particles were made using a 0.01 molar and a 0.001 molar solution of gold chloride ($HAuCl_4{\cdot}H_2O$) in ethanol respectively. The solution was dispensed onto the substrate before the sample was spun at a frequency of 5000 rpm. Calcination of the samples was carried out at 450°C for 4 hours, and a temperature ramp of 5°C per minute. All samples were made from pieces of a single silicon wafer with an artificially grown oxide layer of 394 $\pm$ 3 nm according to the specifications of Philips.

Large gold particles

The first sample (Au06) studied was made with the 0.01 molar solution giving relatively large particles. From optical microscopy it is clear that the particles are homogeneously

distributed over the surface with the smallest visible particles having a diameter of the order of 200 nm. Interference rings can be seen around the particles, making it hard to determine the exact size of the particles. The presence of water in the atmosphere or the solvent is seen from the features shown in figure 5.1. Inside the features, with a diameter of approximately 40 μm there are only a few small particles visible. AFM images from

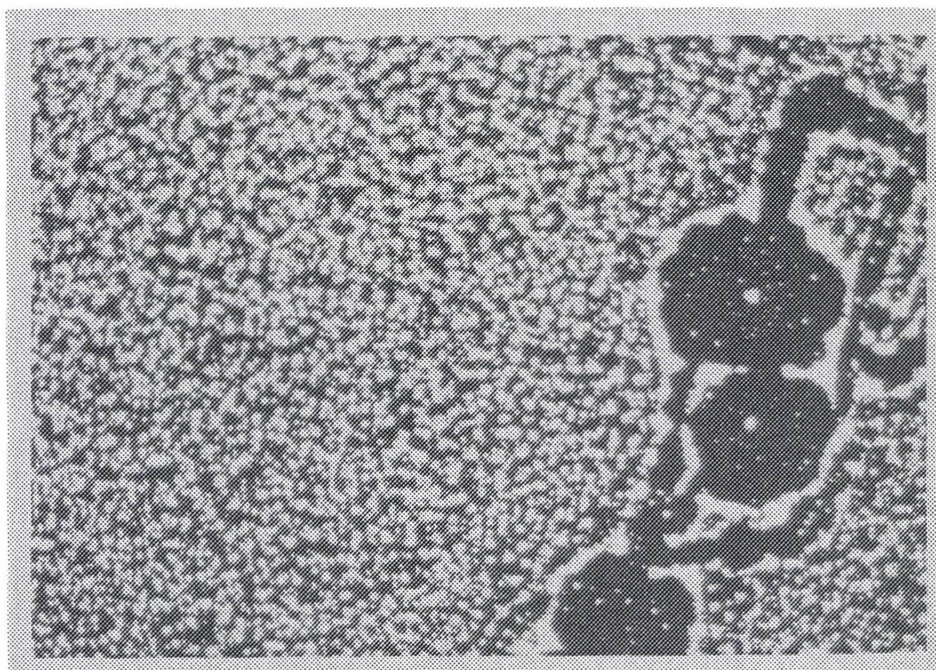

Figure 5.1: *Optical microscopy (dark field) image of sample Au06. The diameter of the circular, nearly empty features is approximately 40 μm. The smallest visible particles are $\approx$200 nm diameter. The particle size appears bigger due to diffraction.*

different areas show particles as small as 60 nm in diameter and 20 nm in height and particles as large as 100 nm in diameter and 40 nm in height. These large ones are the ones seen by optical microscopy. It is clear that two different sizes of particles are deposited of which the small ones are invisible to optical microscopy.

These particles can be compared with the particles on another sample (Au04), prepared in the same way, but on a substrate with 374 nm oxide. SEM images of Au04 show particles of approximately 200 nm diameter as well as micrometer-size particles. Interesting features seen on Au04 are some clusters of small gold particles around micrometer-size particles. The clusters have dimensions in the order of 10 μm and a particle density of more than $3 \times 10^9 \text{cm}^{-2}$ inside the cluster. This is higher than the values obtained from AFM images of Au06 ranging from $3 \times 10^8 \text{cm}^{-2}$ to $2 \times 10^9 \text{cm}^{-2}$. EDX measurements on the particles of sample Au04 show that they are gold particles. However, some of the large particles also contain chlorine.

For the ellipsometry experiments a reference sample was also made which underwent the same heat treatment as Au06. In figure 5.2 the ellipsometric quantities $\tan(\Psi)$ and

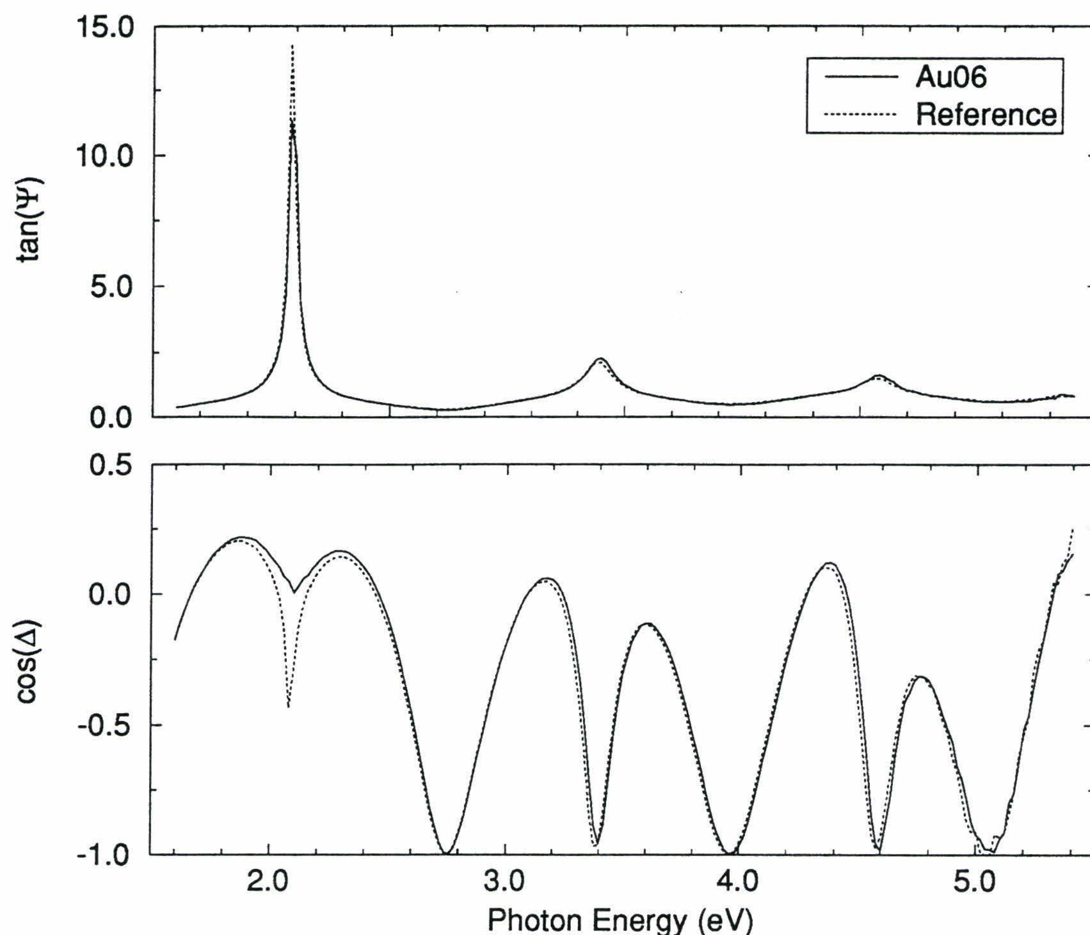

Figure 5.2: *Ellipsometric spectra of the sample with large gold particles, Au06, and the reference sample.*

cos(Δ) are shown for Au06 and the reference sample. From this figure it is clear that the gold has only a minor effect on the spectrum. At the first resonance the error in tan(Ψ) is so large that it is unwise to compare the magnitude of tan(Ψ) for the two samples. It is sufficient to look at cos(Δ) for information about the gold particles. For this reason the tan(Ψ) spectra will not be shown for the other samples.

The difference ($d\cos(\Delta)$) of the cos(Δ) spectra of Au06 and the reference sample gives a better insight into the influence of the particles. This difference spectrum, as shown in figure 5.3, turns out to be nearly identical to the difference between the Au06 spectrum and a simulated spectrum of a 400 nm SiO_2 layer on Si. Apparently the reference sample doesn't have the expected 394 nm oxide layer but a 400 nm thick oxide layer.

To see whether or not it is the gold that causes the difference between spectra of the reference sample and the Au06 sample, simulated spectra of two substrates are compared.

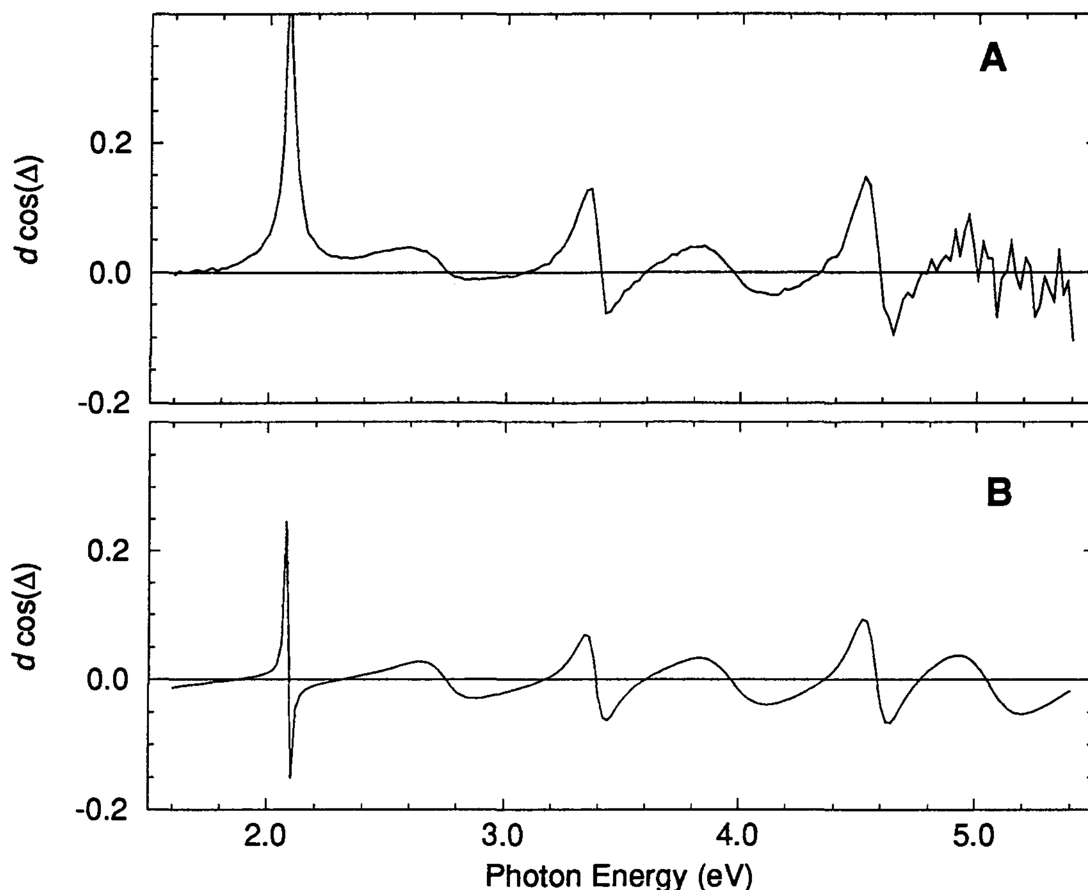

Figure 5.3: A. *Difference of the spectra of the sample with large gold particles, Au06, and the reference sample.* B. *Difference between two simulated spectra of Si with oxide layers of 399 nm and 400 nm respectively.*

The difference between the spectra of samples with a 399 nm and a 400 nm thick oxide layer is identical to that between Au06 and the reference sample, except for the resonance at 2.08 eV, see figure 5.3. From this and the fact that the Au06 spectrum and the simulated spectrum of the substrate with a 399 nm oxide layer differ only significantly at the resonance peak at 2.08 eV it is concluded that Au06 has a 399 nm oxide layer.

The difference between the Au06 minus the 399 nm simulation and the reference sample minus the 400 nm simulation is only evident in the region of the resonance of 2.08 eV. The gold has a wider and higher peak at the 2.08 eV resonance. Unlike the gold difference spectrum, the simulated substrate difference shows a peak *and* a dip near the resonance frequency, indicating a shift of the resonance peak.

Gold monolayer

To check the sensitivity for gold monolayers, a sample has been prepared where approximately one monolayer of gold has been deposited by evaporation (sample Au20). Again the reference sample for this sample (Ref2) does not have the expected oxide thickness of 394 nm but an oxide layer of 400 nm thick. The oxide layer of the Au20 sample itself turns out to be 401 nm thick. The exact position of the resonance cannot be determined from the experiment, since the ellipsometer has a resolution of 0.02 eV. As can be seen from the difference spectrum shown in figure 5.4, the peak at the resonance has a different shape compared to that of the large gold particles. In terms of the cos(Δ) spectra of the monolayer and the large particles, this means that the dip at the 2.08 eV resonance in the monolayer spectrum is steeper than the one in the large particle spectrum. The resonance for the monolayer is at the same energy as the substrate and with the same phase angle Δ, while Δ at the resonance differs 90 degrees with respect to the substrate for the large particles he substrate value. Also the width of the resonance peak in the difference spectra is larger for the large gold particles than for the gold monolayer. The difference

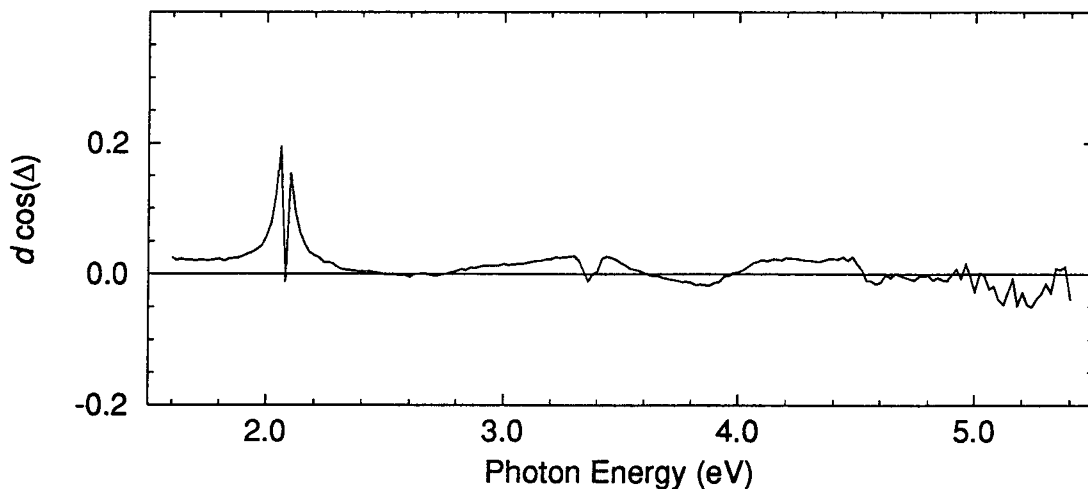

Figure 5.4: *Difference of the spectra of the sample with the gold monolayer, Au20, and the simulated spectra of Si with an oxide layer of 401 nm.*

between the monolayer spectrum and the substrate is sufficient to say that a monolayer can be detected. Fitting the data of the monolayer spectrum to a model system with the *V.A.S.E.* [25] program, resulted in a model with 400.7 nm SiO_2 and a top layer of 0.64 nm modelled with 94% Au and 6% voids. For the toplayer the Bruggeman effective medium approximation is used. The data was converted to Δ and Ψ before the model was fitted.

Small gold particles

The sample with small gold particles, Au11, was made in the same way as Au06, but with a ten times diluted solution. The ellipsometry spectrum (figure 5.5) shows a sample with a 397 nm thick oxide layer. The difference spectrum of Au11 and a simulated substrate with 397 nm oxide is nearly the same as the one for the monolayer of gold minus its simulated substrate. Due to the difference in oxide layer the resonance peak has shifted by 0.02 eV (which is equal to 1 datapoint) from 2.08 eV to 2.10 eV. To compare this result

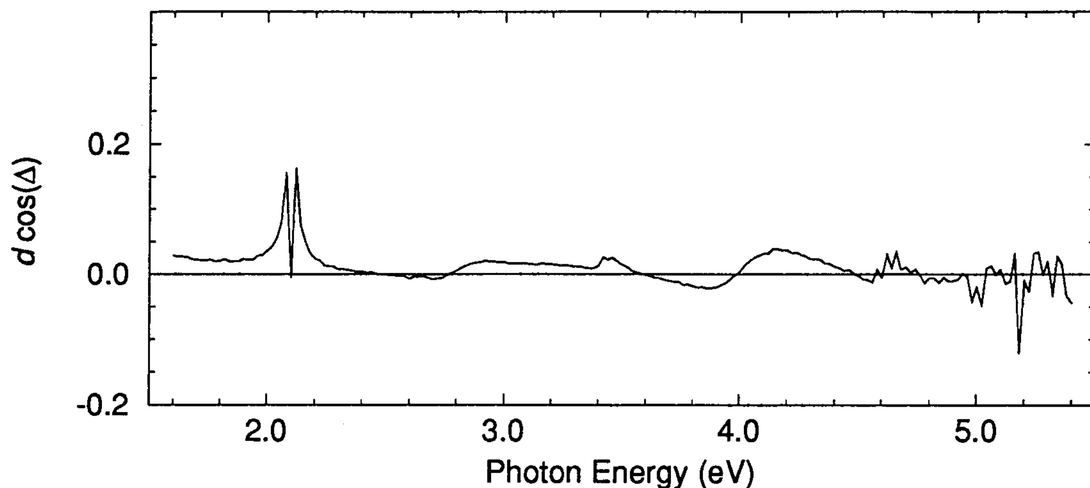

Figure 5.5: *Difference of the spectrum of the sample with the small gold particles, Au11, and the simulated spectrum of Si with an oxide layer of 397 nm.*

with the other two samples, the particle size and distribution have to be known. Optical microscopy images show clustering of particles in the middle of the sample around a large nucleus ($220 \times 150 \mu m^2$) as can be seen in figure 5.6. On the image in figure 5.6*B*, with the same magnification as in figure 5.1 it is seen that the particle density is smaller for this sample than for Au06. However, the particles seen with the optical microscope are much larger than expected from spin-coating parameters and from previous work on small copper particles [29]. AFM images of this sample show particles of the order of 100 nm in diameter and 20 nm in height. The density of these particles is about $1 \times 10^8 cm^{-2}$. These are the particles seen with the optical microscope. Very small particles, with a height between 4 nm and 10 nm and diameters ranging from 20 nm to 90 nm are also present. These small particles have a density of 10^9particles/cm^2. The larger particles, being also present on the sample with large particles, are probably formed in the solution before the spin-coating. Filtering of the solution prior to the deposition is required to remove these particles.

To compare the gold particles with the gold monolayer, the number of gold atoms present in the particles is calculated, assuming hemispherical particles with a radius equal

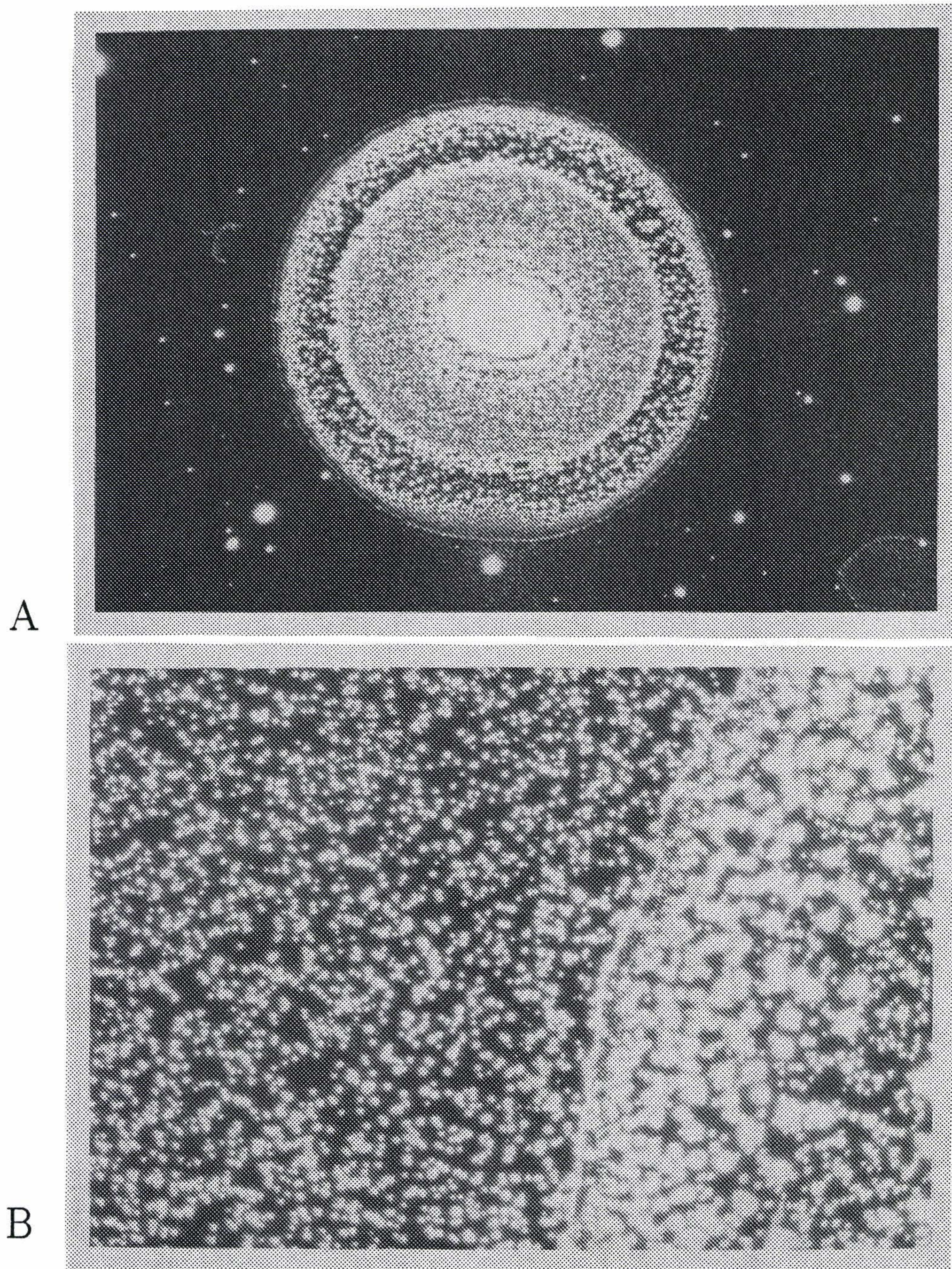

Figure 5.6: *A. Optical microscopy (dark field) image of sample Au11. The feature in the middle has a diameter of approximately 1 mm. B. Enlarged image of the border of the structure shown in A. The small particles are outside the structure.*

to the height of the particles. The load (l) in atoms/cm^2 is then given by

$$l = \frac{2n\pi h^3}{3V}, \tag{5.1}$$

where n is the measured particle number density [cm^{-2}], h the average particle height and V the atomic volume [m^3] (see appendix A). For the large gold particles on sample Au06 this gives a load of 1.0×10^{15} atoms/cm^2 while the particles on Au11 give a load of 1.3×10^{14} atoms/cm^2. If the definition of a monolayer on SiO_2 is taken as $V^{-2/3}$, where V is the molecular volume of SiO_2 (Appendix A), then the amount of gold on Au06 would be enough for 1.25 monolayer, while the gold on Au11 is just enough for 0.15 monolayer.

The fact that ellipsometry suggests the presence of a monolayer of gold for sample Au11 is in disagreement with these AFM results. A closer look at the AFM images hints at a possible explanation. The relatively small height of the particles compared to their diameter suggests that the particles might be higher than the height obtained from AFM. The fact that this is not observed with AFM can be a result of the convolution of the AFM tip and the surface, especially if the distance between the particles is small. AFM images are always a result of the convolution of the tip and the surface as explained in section 4.2.1 and figure 4.1. As an example an AFM line scan of sample Au11 is shown in figure 5.7. With other experimental techniques like Rutherford Backscattering Spectroscopy (RBS)

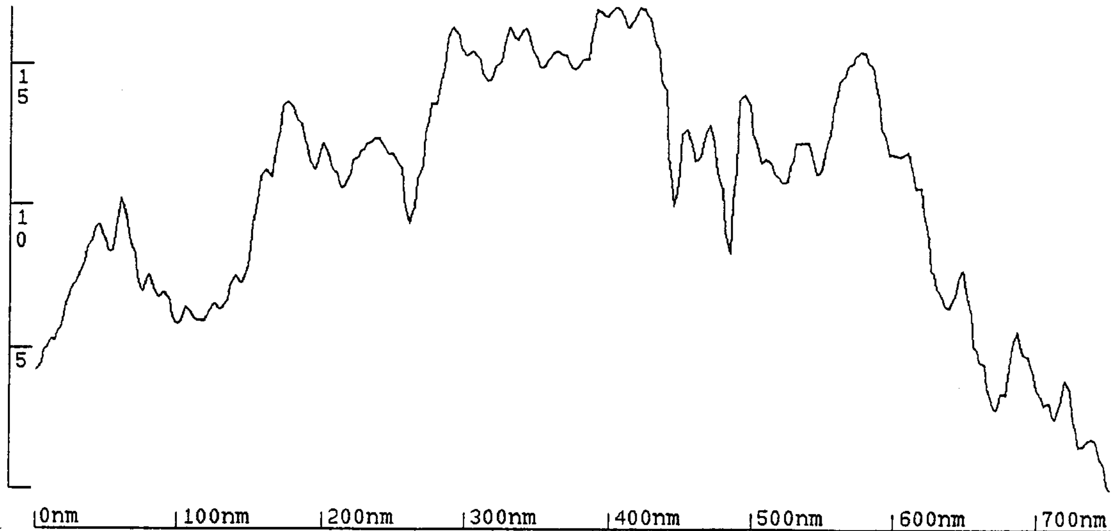

Figure 5.7: *An AFM line-scan of sample Au11.*

the total amount of gold on the sample can be determined which then can be compared with the AFM results. This, however hasn't been done yet.

Discussion

From the experiments on the gold monolayer it is clear that thin gold layers are detectable with spectroscopic ellipsometry. Determination of the effective dielectric function of the gold-monolayer is not possible [33]. Direct comparison with literature is thus not possible, but measurements on thin films can be compared qualitatively with measured spectra. The dielectric function of a gold film (100 Å to 250 Å thick) reported by Palik [22] shows a shoulder in its real part around 2 eV. However, measurements by Jans [33] on a thin gold layer do not show this feature. The results for the gold monolayer also show no plasmon specific features.

Comparing this with the results for the large gold particles, the peak at 2.08 eV is noted for the large gold particles. In literature several values for the Mie resonance of gold particles are reported. Kreibig [32] and Zhou [3] report values of 2.34 eV for particles with a diameter in the range of 6 nm to 40 nm. The full halfwidth of this resonance peak is estimated to be of the order of 0.4 eV and decreases with increasing particle size [14]. The resonance in the ellipsometry spectra due to the SiO_2 thus doesn't have to be *exactly* at the same energy as the Mie resonance to allow for detection. From these measurements the exact Mie resonance frequency cannot be determined. However, one can say that the resonance is present since a strong contribution is seen around 2.08 eV while the rest of the spectrum can be explained by a difference in the oxide layer.

For the small gold particles one can clearly conclude that the Mie resonance is not present. The optical behaviour is very similar to that of the gold monolayer.

There are three possible reasons for the absence of the plasma resonance. The first reason could be a shift of the resonance peak outside the spectral region studied. This, however, is rather unlikely when shifts of the Mie frequency and the width of this resonance reported in literature are considered. Kreibig [32] for example, reports a shift of only 0.14 eV when the particle diameter is decreased from 6 nm to 2.5 nm.

A second reason is that if the particles are too small, the electrons will be localised (or the conduction band will break into discrete levels) and collective oscillations are no longer possible.

AFM measurements give no conclusive results about the particle size and separation for the very small particles. If the particles touch and form a thin film, this film cannot be recognised by the AFM as being gold. Only the particles sticking out of this layer are seen, which would account for the relative small height compared to the diameter of the smallest particles detected.

The third possible reason for not detecting plasmons is the formation of such a thin gold film, instead of particles. Due to the used deposition technique, this thin film would be of the order of a monolayer thick, which would explain the similarity between this spectrum and the monolayer spectrum. The fact that a feature is seen near the plasma resonance in the data of Palik [22] and not in this data can also be caused by the fact that in Paliks case the gold layer is much thicker (100-250 Å). Conduction (or *sp*) electrons are more localised

at a surface than in the bulk. In layers of the order of a monolayer, the atoms are at an interface at two sides and the localisation of the conduction electrons will be stronger than at the surface of a thick layer. In fact the localisation might even be so strong that similar effects can occur as expected for very small particles, where the energy bands break up and collective excitations are no longer possible.

Conclusions

Concluding one can say that the Mie resonance is present for the large gold particles, but not for the small gold particles and the gold monolayer. The absence of the resonance for the small particles might be due to their size. The similarity with the monolayer spectrum however, suggests that the small particles have formed a thin film. The fact that the Mie/plasma resonance is not seen for the small particles *and* the monolayer suggests that similar processes of localisation of conduction electrons is the reason for this absence. Additional surface studies of the sample with small gold particles are necessary to determine whether these particles have formed a film or not.

5.2 Copper particles

Two different procedures were used for the preparation of copper particles. All copper samples were deposited on silicon with an oxide layer quoted to be 394 nm. This silicon wafer is the same one as that used for the gold particles.

The large copper particles were deposited using a 0.053 wt% solution of $Cu(NO_3)_2 \cdot H_2O_{2.5}$ in cyclohexanone as suggested by Kuipers *et al.* [28,30]. Spin frequencies ranged from 735 rpm to 2060 rpm. During spin-coating the glovebox is purged with N_2 to enhance the evaporation of the cyclohexanone. After spin-coating the samples were dried in air for 20 minutes at 50°C and for another 20 minutes at 100°C. Finally they were calcined at 300°C for 1 hour. The temperature was increased at a rate of 5°C/minute. Reduction was at 200°C in 60 mbar H_2 for one hour with the gas being refreshed continuously.

The small copper particles were deposited as described by Toussaint [29], using a 0.01 molar solution of copper(II)acetate ($Cu(ac)_2 \cdot H_2O$) and a spin frequency of 5000 rpm. Calcination was done at 450°C for 4 hours, with a temperature ramp of 5°C/minute.

Optical microscopy images of the large particles showed nearly empty areas with only a few particles ($\sim$ 2mm^{-2}) present. The particle density is even lower in the middle of the sample. The particles were too large for the AFM in the Surface and Interface Physics group, which has a maximum vertical scale of 280 nm. The AFM present in the group of prof. v. Santen in the chemistry department is a Topometrix, TMX 2000, which can scan areas up to 75 $\times$ 75 μm^2 and has a maximum vertical range of several micron. Two of the large particle samples (Cuo21 and Cuo24) were studied with this AFM. Large clusters, with a characteristic diameter of 18 μm and a height of 80 nm are visible on both samples as is shown in figures 5.8 and 5.9. Increasing the magnification, going from A to D the particles in the clusters become visible. These particles are approximately 220 nm in

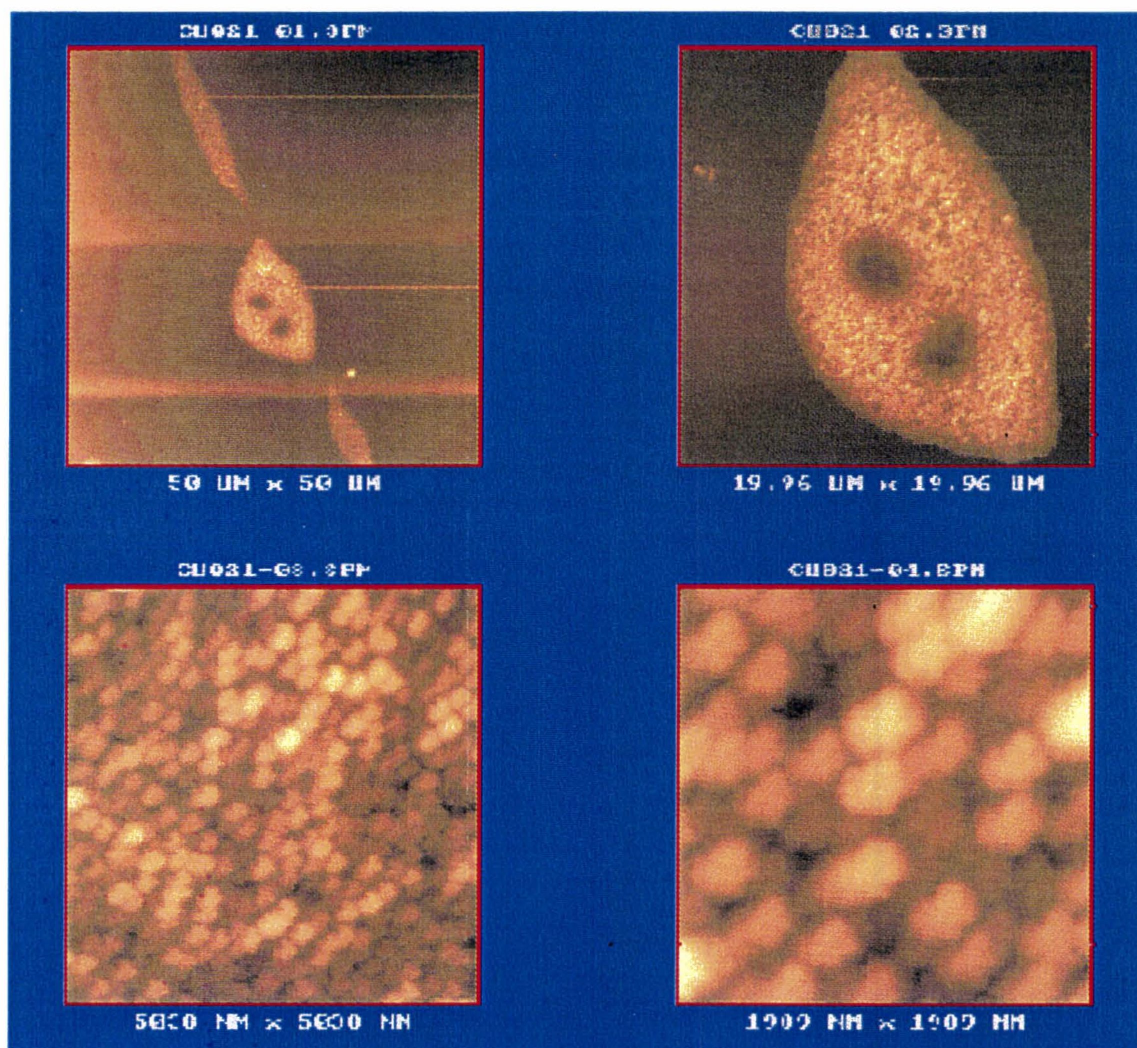

Figure 5.8: $^{AB}_{CD}$ *AFM images of Cuo21. The scanned areas are* 50×50 μm^2, 19.96×19.96 μm^2, 5.038×5.038 μm^2 *and* 1.989×1.989 μm^2 *for figure* A, B, C *and* D *respectively.*

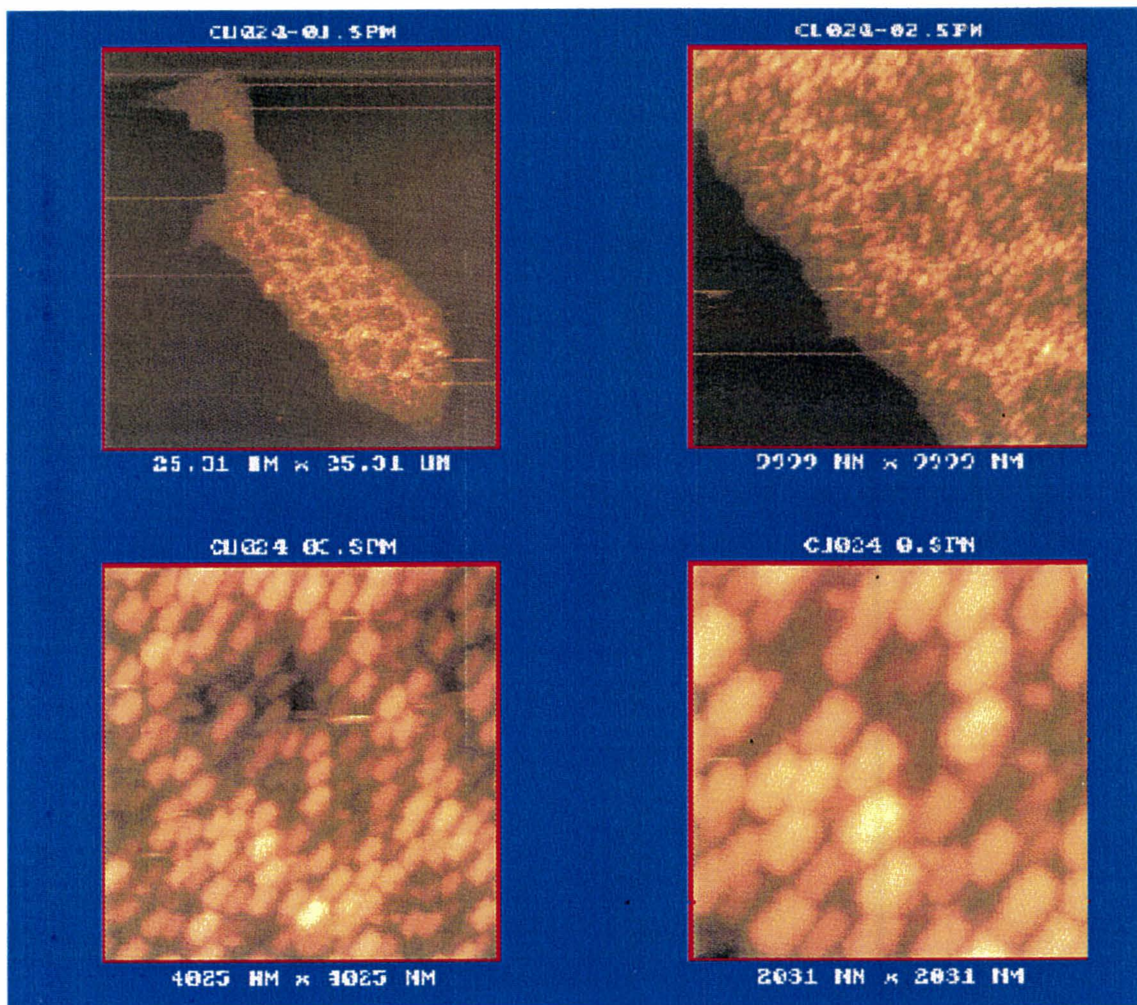

Figure 5.9: $^{AB}_{CD}$ *AFM images of sample Cuo24. The scanned areas are* $25.31 \times 25.31\ \mu m^2$, $9.999 \times 9.999\ \mu m^2$, $4.025 \times 4.025\ \mu m^2$ *and* $2.031 \times 2.031\ \mu m^2$ *for figure* A, B, C *and* D *respectively.*

diameter and 20 nm in height, according to these images. However, like the AFM images of the small gold particles, here too, the convolution of tip and surface has its effect on the image. The particles all appear to have approximately the same size, which suggest that the observed particle size tells actually more about the tip size than about the particles. The particles have a maximum diameter of 220 nm, as is seen in the figures 5.8*D* and 5.9*D*, but are probably smaller. There is no real difference to be seen between Cuo21 and Cuo24, although they were prepared with different spin frequencies: for sample Cuo21 a spin frequency of 735 rpm was used, while Cu24 was spun at 2060 rmp.

The samples with the small copper particles appear to be completely empty when seen through an optical microscope. This means that the particles are all smaller than 100 nm or are not present. AFM images show indeed a high concentration ($\sim 1 \times 10^{10}$ particles/ cm^2) of particles on the surface with an average diameter of 50 nm and a height ranging from 5 to 15 nm. This particle number concentration is in agreement with [29], but the particle diameter is about three times too large. The large particle diameter and the fact that all particles have approximately the same, nearly rectangular, shape suggests that the used AFM tip is too blunt for nanometer scale images.

The samples used for ellipsometry, including the reference sample, were reduced in H_2 at 200°C for 1 hour prior to the ellipsometry experiments. The temperature ramp was again 5°C/min. After reduction, the samples were kept in a nitrogen atmosphere and mounted on the sampleholder inside a glovebox with an argon atmosphere (<1 ppm O_2 and < 1 ppm H_2O). A suitcase with nitrogen atmosphere was used to transport the samples to the experimental setup. During the ellipsometry experiments, the sampleholder is flushed with nitrogen to prevent the sample from oxidising.

For the three samples studied, the spectra minus the reference spectrum are shown in figure 5.10. For sample Cuo24 it is clear that there is no difference between this sample and the reference sample. The spectra of Cuo25 and Cuo27 are identical and can be explained by assuming a difference in the oxide layer thickness of these two samples and the reference sample.

Discussion

Several reasons are possible for the absence of a Mie resonance in the spectra of the copper particles. It is possible that the copper particles were oxidised. Though the procedure to prevent oxidation worked well in other situations [33], there is no guarantee that it works well for copper. For the small copper particles, this is a good argument, since they are so small that they will oxidise completely and oxidised copper has no plasma resonance. It is, however, no good argument for the large copper particles, since they would *not* oxidise completely. A Cu_2O shell will form around a large Cu-core. Such a structure still shows a plasma absorption [34].

The reverse structure, with a Cu shell on a Cu_2O core is also possible if the particles are not completely reduced. This too is no good argument, since it is has been shown both theoretically and experimentally that metal-coated nanoparticles exhibit these absorptions as well [1].

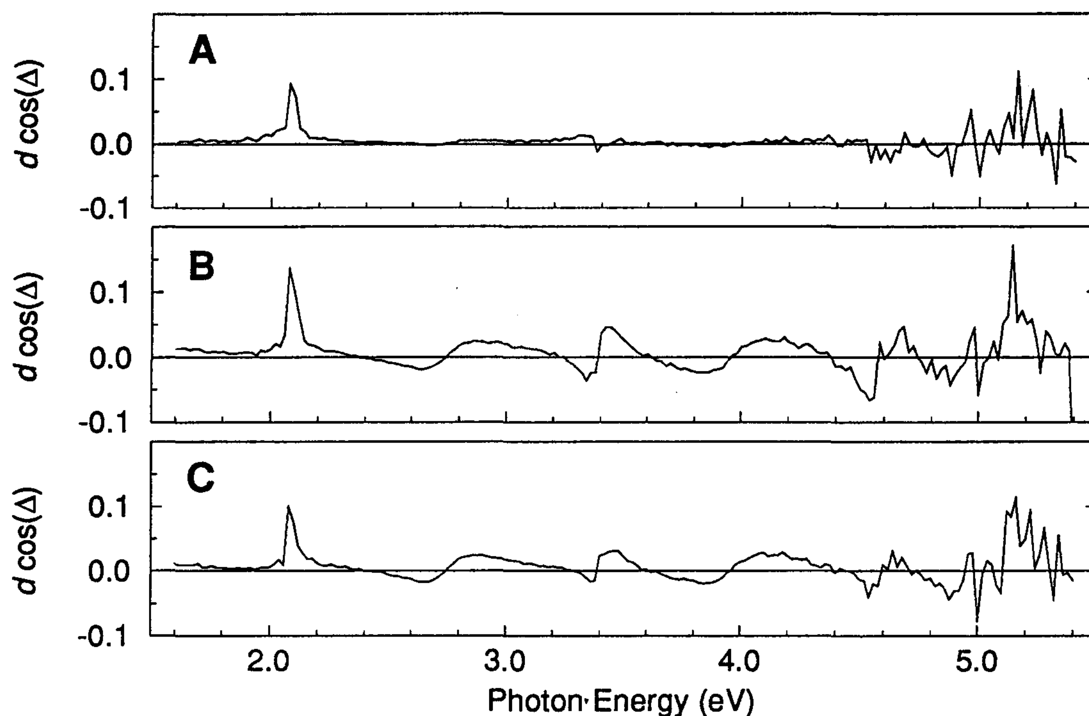

Figure 5.10: *Ellipsometry spectra of the samples studied minus the spectrum of the reference sample. Samples Cuo24 (A) and Cuo25 (B) have large clusters of copper particles, while sample Cuo27 (C) has small copper particles.*

The total amount of copper present for the large particles, is at most 0.5 monolayer if the same procedure is used to calculate the coverage as in the case of the gold particles. The number of clusters per cm^2 near the side was used to calculate this coverage. In the center of the sample, where the ellipsometry experiments were done, the amount of copper present is even much less, because most copper has moved towards the sides during the sample preparation. This, and the fact that there is nearly no contribution at all of the copper to the ellipsometry spectra, suggests that the copper coverage is too small to be detected.

For the small copper particles localisation of the electrons is another possible reason for the absence of the Mie resonance. As in the case of gold particles, the conduction band can break up into discrete levels when the particles become very small, which means that the conduction electrons are localised. But even before the conduction band breaks up, localisation effects can occur. At a metal surface, band narrowing of the *sp*-bands occurs. Photoemission experiments on small copper particles [35] show a further narrowing of the *sp*-bands when the particle size is decreased from 50 nm to 5 nm diameter. This is schematically shown in figure 5.11. For copper the centre of the *sp*-band lies below the

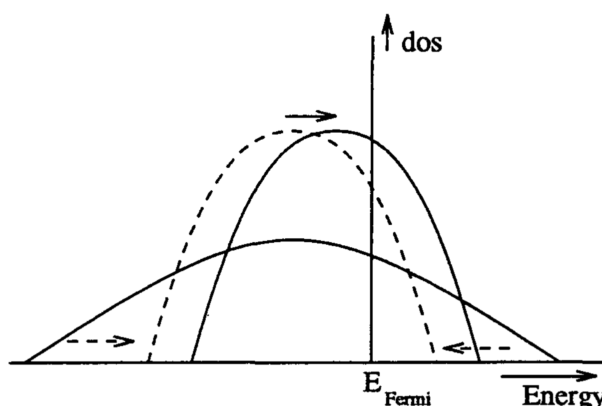

Figure 5.11: *Schematic representation of the narrowing and shift of the sp band.*

Fermi level and a narrowing of the band thus means that more electrons will be present in the *sp*-band. Metals however will keep the surface neutral, so that the centre of the *sp*-band has to move towards the Fermi level. The electrons are now even more localised, because the part of the *sp*-band below the Fermi level has become smaller and the *sp*-band is further away from the *d*-band. If the localisation is strong enough, collective oscillations of the electrons are not possible anymore and Mie resonances will not be observed.

Conclusions

For the large copper particles the conclusion is that there is not enough copper on the sample to detect copper or its resonances. Oxidation of the particles is for the large particles no reason for the absence of the Mie resonance. For the small copper particles, oxidation is one possible reason for the absence of the Mie resonance. Another reason is the localisation of the electrons, possibly due to the narrowing and shift of the *sp*-band.

5.3 Recommendations

Although AFM works fine for the determination of particle size and distribution of most samples it is suggested to use STM to determine the particle size and distribution as well as Rutherford Backscattering Spectroscopy to determine the total amount of metal deposited, for small metal particles.

Experiments and reduction of the sample in a UHV system are suggested to eliminate the oxidation of the particles after reduction. With the ellipsometer present in the Surface and Interface Physics Group, it is possible to do ellipsometry in a UHV environment. Evaporation deposition is also possible on this system, so that *in situ* ellipsometry can be done while particles are grown.

The use of other solvents for the spin-coating of large copper particles is recommended. Since $Cu(NO_3)_2 \cdot H_2O_{2.5}$ is very hygroscopic, the preparation of samples with this precursor should be done fast and in a low humidity environment. Cyclohexanone does not evaporate quickly and is very viscous, which enhances the formation of large clusters of particles. Faster evaporating solvents like butanol or ethanol are therefore suggested.

With the ellipsometer at the Philips Research Laboratories it is possible to do Variable Angle Spectroscopic Ellipsometry (VASE), which gives more information about the particle contribution to the spectrum. Changing the angle of incidence, the resonance due to the oxide layer will shift to other energies, while the plasma resonance remains at the same energy. The only disadvantage of this technique is the relatively long time it takes to do the experiment (approximately one hour per spectrum at fixed angle), enough to allow the sample to oxidise. Using the gold particles and the special sampleholder that can be flushed with N_2, this effect can be minimised.

A final point that deserves attention is consideration of the substrate. Since the wafers are not homogeneous, it is difficult to compare different samples. The in-situ ellipsometry during evaporation deposition elliminates this problem. VASE experiments also make it easier to determine the oxide layer thickness. Taking an ellipsometry spectrum of the substrate before deposition of the particles gives the oxide layer thickness. This spectrum is not good enough however to subtract it from the spectrum with the particles on the sample, because the ellipsometer becomes very sensitive to misallignment when using the resonance method. This is already clear when spectra taken at a polariser angle of $+20°$ and $-20°$ are compared. If the callibration hasn't been done accurately enough, the dip in $\cos(\Delta)$ at the first resonance can be present at $-20°$ and can be gone at $+20°$.

References

[1] J.W. Haus, H.S. Zhou, S. Takami, M. Hirasawa, I. Honma, and H. Komiyama, J. Appl. Phys. **73**, 1043 (1993).

[2] A. Wokaun, J.G. Bergman, J.P. Heritage, A.M. Glass, P.F. Liao, and D.H. Olson, Phys. Rev. B **24**, 849 (1981).

[3] H.S. Zhou, I. Honma, H. Komiyama, and J.W. Haus, Phys. Rev. B **50**, 12052 (1994).

[4] J.D. Jackson, *Classical Electrodynamics*, second edition, John Wiley & Sons, New York (1975).

[5] M. Born and E. Wolf, *Principles of Optics*, sixth edition Pergamon Press, Oxford, New York (1985).

[6] F. Wooten, *Optical properties of solids*, Academic Press, New York and London (1972).

[7] M.Rocca, Surf. Sci. Rep. **22**, 1-71 (1995).

[8] C.F. Bohren and D.R. Huffman, *Absorption and Scattering of Light by Small Particles*, John Wiley & Sons, New York (1983).

[9] T. Reiners, C. Ellert, M. Schmidt, and H. Haberland, Phys. Rev. Lett. **74**, 1558 (1995).

[10] J. Tiggesbäumker, L. Köller, K.-H. Meiwes-Broer, and A. Liebsch, Phys. Rev. A **48**, R1749 (1993).

[11] K.-P. Charlé, W. Schulze, and B. Winter, Z. Phys. D **12**, 471 (1989).

[12] Y. Borensztein, P. De Andrés, R. Monreal, T. Lopez-Rios, and F. Flores, Phys. Rev. B **33**, 2828 (1986).

[13] U. Kreibig and L. Genzel, Surf. Sci. **156**, 678 (1985).

[14] S. Holst and W. Legler, Z. Phys. D **25**, 261 (1993).

[15] R.M.A. Azzam and N.M. Bashara, *Ellipsometry and Polarized Light*, North Holland, Amsterdam (1977).

[16] R.W. Collins, Rev. Sci. Intrum., **8**, 2029 (1990).

[17] E. Hecht, *Optics*, second edition, Addison–Wesley publishing company, London (1987).

[18] G.M.W. Kroesen, Lecture notes (1994).

[19] R.M.A. Driessens, Master thesis, Physics Department, TU Eindhoven (1994).

[20] J.B. Theeten, D.E. Aspnes, and R.P.H. Chang, J. Appl. Phys. **49**, 6097 (1978).

[21] J.C. Jans and J.W. Gemmink, Appl. Opt. **32**, 84 (1993).

[22] E.D. Palik, *Handbook of optical constants of solids*, 2 volumes, Academic Press, New York and London (1985,1991).

[23] J.C. Jans, Philips J. Res. **47**, 347 (1993).

[24] D.E. Aspnes and A.A. Studna, Appl. Opt. **14**, 220 (1975).

[25] Johs Blaine, *V.A.S.E. for MS-Windows^{tm}*, version 1.60, J.A. Woollam Co., ©1991, 1992.

[26] J.M.M. Nijs, A.H.M. Holtslag, A. Hoekstra and A. van Silfhout, J. Opt. Soc. Am. A, **5**, 1466 (1988).

[27] A. Partridge, S.L.G. Toussaint, and C.F.J. Flipse, to be published.

[28] C. Doornkamp, C. Laszlo, W. Wieldraaijer, and E.W. Kuipers, J. Mater. Res. **10**, 411 (1995).

[29] S.L.G. Toussaint, Master thesis, Physics Department, TU Eindhoven (1994).

[30] E.W. Kuipers, C. Laszlo, and W. Wieldraaijer, Cat. Lett. **17**, 71 (1993).

[31] U. Kreibig, Solid State Commun. **28**, 767 (1978).

[32] U. Kreibig, J. Physique **38**, C2–97 (1977).

[33] J.C. Jans, Private communications.

[34] H. Hosono, Phys. Rev. Lett. **74**, 110 (1995).

[35] C.F.J. Flipse, Private communications.

Dankwoord

Na zes mooie jaren komt er nu dan toch een (voorlopig) einde aan mijn verblijf in het Brabantse land. Maar voordat ik weg ga wil ik op deze plaats eerst nog de mensen bedanken die me met raad en daad hebben bijgestaan tijdens mijn afstuderen.

Op de eerste plaats wil ik mijn direkte begeleider Kees Flipse bedanken voor de prettige samenwerking en de vele kansen die hij me gegeven heeft, ook voor na mijn afstuderen. Zijn nimmer aflatend enthousiasme zowel binnen als buiten de fysica blijft een bron van inspiratie. Professor Brongersma wil ik graag bedanken voor de gelegenheid die hij mij geboden heeft om een half jaar in Dublin te mogen proeven aan de Ierse fysica (en aan andere Ierse dingen), om deze daarna te vergelijken met de fysica binnen de groep FOG.

Ruim een half jaar lang heb ik de geheimen van de electronica en het leven mogen leren van Rein Rumphorst. Dit was een zeer prettige samenwerking waar ik nog vaak met plezier aan zal terugdenken. Systeem-beheerder en electronicus Wijnand Dijkstra en technicus Gerard Wijers wil ik graag bedanken voor de technische ondersteuning. Verder wil ik alle mensen binnen de groep FOG bedanken voor de prettige samenwerking. Hierbij wil ik speciaal Alan Partridge en Ronald van den Oetelaar bedanken voor de AFM experimenten.

I want to thank Des O'Mahony for the helpfull discussions we had about physics and a lot of other things, the pleasant times we had both in Eindhoven and in Dublin and for introducing Calvin and Hobbes to me. I would also like to thank Marielle Fontaine-Carrère for her help and interest.

Buiten de groep FOG gaat mijn hartelijke dank naar M. Hendrix voor de SEM experimenten en naar P. Gunter voor de AFM experimenten. Binnen de TUE wil ik verder nog graag al die mensen bedanken waarvan ik apparatuur heb mogen gebruiken. Met name noem ik hier Hans Dalderop bij Vaste Stof fysica en D. Klepper en J.v. Grondelle bij de faculteit Scheikundige Technologie.

Buiten de TUE wil ik graag Jan Jans op het PRLE (Philips NatLab voor gewone mensen) bedanken. Behalve dat het erg prettig samenwerken was, waren er door zijn gastvrijheid en hulp toch nog ellipsometrie experimenten mogelijk.

Studeren is niet alleen op de TUE werken, maar ook wonen in een gezellig studentenhuis. Jaco, Marion, Mischa, Muriel en Rob bedankt !!!!

En "last but not least" gaat mijn speciale dank uit naar mijn ouders en grootouders, die me altijd in vele opzichten gesteund hebben.

Olaf, juli 1995.

Appendix A

Approximation of the molecular volume

The molecular volume or atomic volume has been used for the calculation of the dispersion or the deposited amount of metal. As an approximation of the molecular volume the following equation has been used:

$$V = \frac{M}{\rho \cdot N_A}, \tag{A.1}$$

where V is the molecular or atomic volume [m^3/molecule or atom], M is the molecular or atomic weight [g/mol], ρ is the density [g/m^3] and N_A is the number of Avogadro which is $6.02 \cdot 10^{23}[mol^{-1}]$.

As an estimation of the interatomic distance or the thickness of one monolayer $a = V^{1/3}$ is used. The molecular or atomic surface density can now be approximated by $V^{-2/3}$. In table A.1 these quantities are listed for gold, copper and SiO_2 [29, appendix C].

Table A.1: *Estimated molecular volumes (V), surface density ($V^{-2/3}$) and monolayer thickness ($V^{1/3}$).*

	ρ [kg/m^3]	M [g/mole]	V [$10^{-29}m^3$]	$V^{-2/3}$ [10^{15} cm^{-2}]	$a = V^{1/3}$ [Å]
Cu	8960	63.64	1.18	1.93	2.28
Au	19300	192.00	1.65	1.54	2.55
SiO_2	2300	60.06	4.34	0.81	3.51